Canadian Journal of Earth Sciences

OPEN ACCESS | Research Article

Characteristics of the Albian Westgate Formation polygonal fault system

Andy St-Onge

PFS Interpretations Ltd., Calgary, AB T2M 2K7, Canada

Corresponding author: **Andy St-Onge** (email: geophysicist@shaw.ca)

Abstract

Borehole logs and 3D seismic data are used to determine the characteristics of a polygonal fault system (PFS) in the Albian Westgate Formation in western Saskatchewan and eastern Alberta. The basal Upper Cretaceous formation is a siliceous siltstone to mudstone deposited in the Western Interior Seaway beneath the Great Plains of North America. The faulted zone is layerbound within the ~80 m thick Westgate Formation at Swift Current, Saskatchewan. Most faulting occurs along grabens approximately 125 m wide and 10 m deep. The grabens are interconnected, have random strike directions, and lengths up to 800 m. The continuous depositional environment of the Westgate Formation enables timing and compacted sediment thickness estimates for the PFS initiation. The faults appear to have started in ~15 m or more of compacted sediment within the first 270 000 years of the 1.5 Myr Westgate Formation interval. Polygonal faulting may result from smectite illitization, subsequent bed dissolution, and polygonal fault formation in overlying beds. Mapping the seismic data in intervals above the Westgate shows relief above the graben through Santonian time. Interpreting the seismic dataset and accompanying wellbore data has resulted in a simple model of graben formation post-Turonian time that could induce fracturing in shallower Second White Speckled Shale Formation strata. Wellbore data interpretations from Alberta and Saskatchewan show that the PFS identified at Swift Current may range across a large area. The implications for an extensive PFS identification in the Lower Cretaceous Westgate Formation and homotaxially equivalent Mowry Shale across central North America are discussed.

Key words: polygonal fault system creation, Albian Westgate Formation, smectite illitization, shear-thinning, shear-thickening, hard-sphere densification

Introduction

Polygonal fault systems (PFSs) are layer-bound normal faults and fractures that form in fine-grained sediments early after deposition. Interpretation using 3D seismic data, especially on continental margins, has identified PFS in over 100 basins worldwide (Cartwright 2011). The faulting can occur shortly after deposition without external stress (Dewhurst et al. 1999; Cosgrove 2001; Cartwright et al. 2007). The faults start in the fine-grained sediments and continue to grow, with their coalesced fault traces resembling polygons in plan view.

Cartwright and Dewhurst (1998) summarized the characteristics of PFS identification. The normal faulting is layer-bound with undisturbed strata above and below. The faulting can occur over areas up to 1000 000 km^2 or more (St-Onge 2017). Individual faults can have up to 100 m vertical offset with 100–1000 m inter-fault spacing. Sometimes, the faulting is observed in two or more tiers of strata, where each tier can have independent fault offsets and geometries. Sometimes, prevalent faults from a lower tier can influence faulting in the upper tier(s).

Various processes have been ascribed to explain PFS development. Historically, normal faulting is thought to start when fluid in a fine-grained hydrated sediment system dewaters (Cosgrove 2001). Several explanations have been proposed for dewatering. For example, syneresis, the spontaneous contraction of a gel without evaporation, has been proposed (Cartwright and Lonergan 1996); however, syneresis cannot account for PFS formation at deeper depths (Goulty and Swarbrick 2005). Sediment density inversion with depth (Goulty 2008) and formation overpressure (Roberts et al. 2015) have been examined as causes of fracture initiation. However, there are limitations to either of these being considered a single initiator for all PFSs.

The work presented here results from 10 years of researching strata across the Western Interior Seaway (WIS) using seismic data, outcrop analyses, and information from wellbores drilled to deeper targets. The work produced two new and novel ideas that will be discussed here regarding the initiation and propagation of a PFS in the Albian Westgate Formation. First, some volcanogenic strata have shear-thinning and/or shear-thickening rheologies. When some volcanogenic strata are sheared, their rheology could mean that the fluid strata can thin or thicken under the shearing force. Simple changes in these rheologies can explain polygonal faulting in some areas (St-Onge 2024, under review). Shear-

Fig. 1. The Westgate Formation (shaded area in Canada) is preserved within the outline of sediments deposited within the Western Interior Seaway (Leckie et al. 2000). The three study areas are shown at Success and Dollard, Saskatchewan, and Marie Lake, Alberta. The Westgate Formation outcrops at Stony Plains, Alberta. Homotaxially equivalent strata are the Mowry Shale and the Shell Creek Shale in the USA (McNeil and Caldwell 1981). The Westgate Formation type section is at National Mills, Manitoba (McNeil and Caldwell 1981; TGI Williston Basin Working Group 2008).

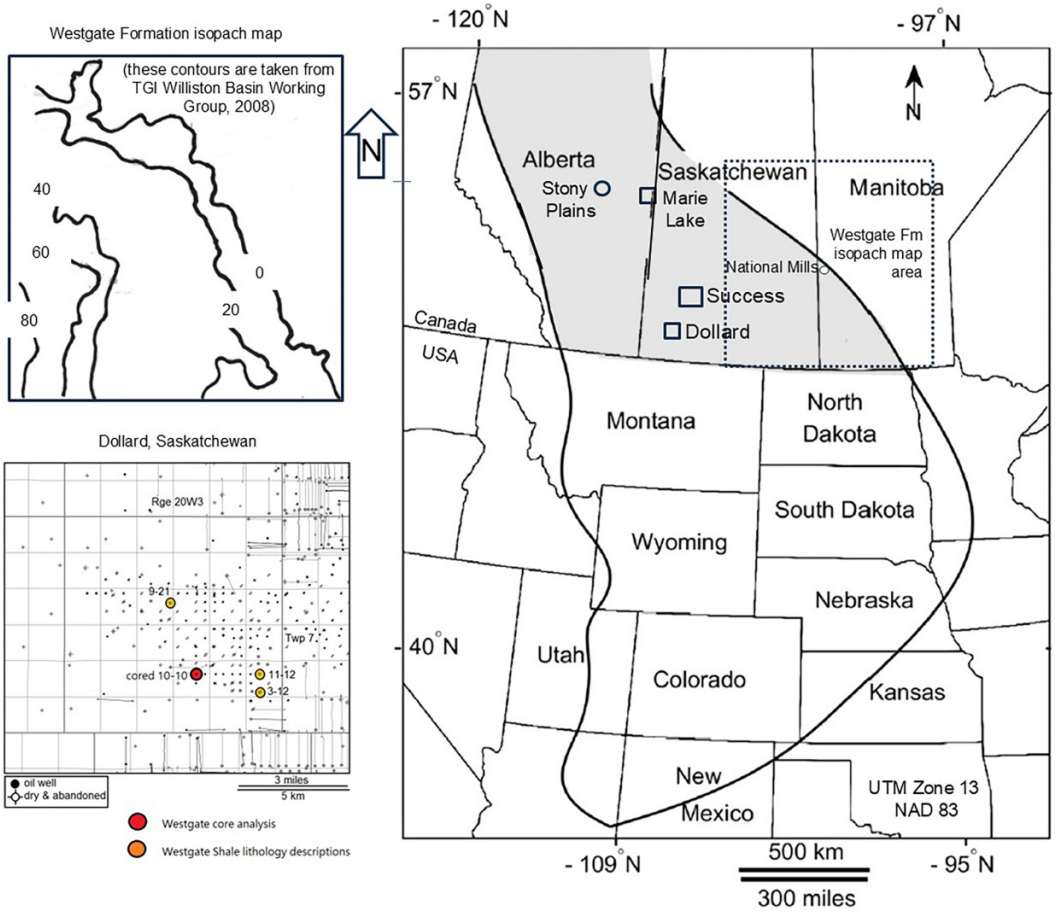

Table 1. Stratigraphic nomenclature and lithologic descriptions for strata in this study.

Most of the observed lithology for this study is fine-grained, volcanogenic strata						
Epoch		Formation	Age	Picks (Ma)	Success, Sask. Elavatlon m*	Lithology (after Bloch et al. (1993) and Christopher et al. (2006))
Upper Cretaceous	Milk River			83.6		
			Santonian	86.3	75	
		Niobrara	Coniacian	89.8	25	Argillaceous shale
		Carlile	Turonian			Bioclastic calcarenite, marlstone, shale
	Colorado Group	2WS		93.9	7	Calcarenite, marlstone, shale, bentonites
		Belle Fourche				Mudstone to siltstone, bentonites
		Fish Scales	Cenomanian	100		Claystone to mudstone, basal sandstone, bentonites
Lower Cretaceous		Westgate	Albian			Claystone to siltstone
		Vikng				Coarsening upward fine sandstone
		Joli Fou				Noncalcareous shale, silstone, and bentonite interbeds

Note: 2WS, Second White Specks.
*Depths are taken from vertical well control located at 50.4650N, −108.1099W.

Fig. 2. The base map for the Success, Saskatchewan area. There were 128 wells analyzed within the bounds of the Greater Success area. TGS Ltd. provided the Leinan and Success seismic surveys. Correlation throw curves for the two well pairs at 12(a), 12(b), and 12(c) are shown in Fig. 4.

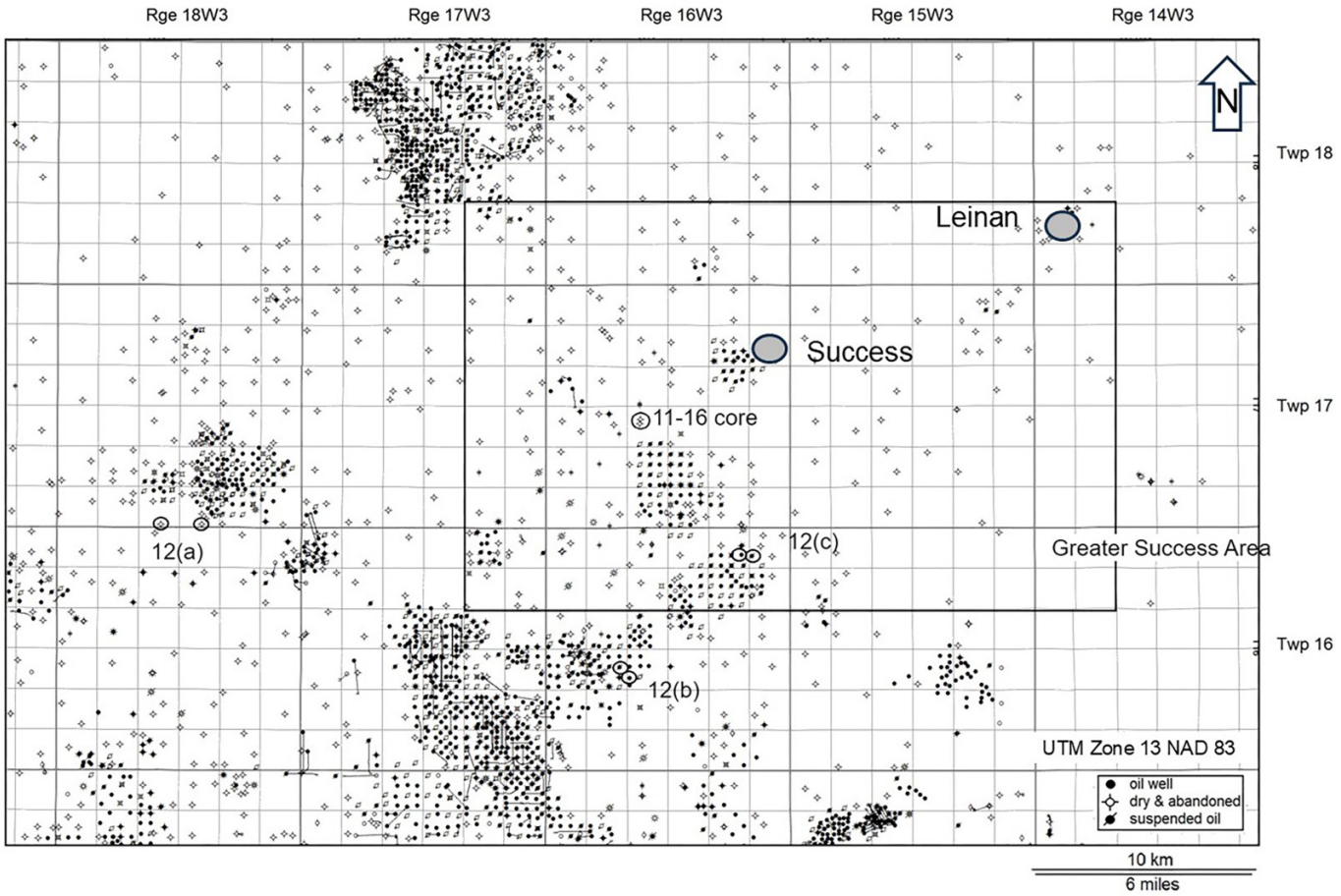

thickening rheology in response to impending earthquake energy can jam and solidify strata as water is displaced. Subsequent shear-thinning of deeper strata can occur. For example, increased potassium concentrations in water can transform shear-thickening smectite into shear-thinning illite (Jeong et al. 2012). This change can happen at shallow depths and cause weakness and bed dissolution, resulting in PFS initiation and propagation, as St-Onge (2024, under review) discussed. Second, the densification of hard-sphere colloidal silica concentrations in Upper Cretaceous strata in the WIS has also been presented as an explanation for PFS development (St-Onge 2024, under review). Gelled silica suspensions can undergo an elastic to brittle transformation when SiO_2 particle volume fractions exceed ~60%. This densification can lead to arcuate polygonal faulting, as observed at the base of a large Upper Cretaceous PFS in southeast Saskatchewan and southern Manitoba (St-Onge, under review).

This paper describes extensive faulting in fine-grained mudstones, siltstones, and bentonitic shales of the Albian Westgate Formation observed in southwest Saskatchewan and central eastern Alberta, which may extend over a substantially larger area. All the fault characteristics are consistent with other PFSs. Seismic data and well-log interpretation date the fault timing to sometime after 270 000 years of the Westgate Formation sediment deposition in ~15 m or more of compacted sediment thickness. A simple isopach analysis of correlative Westgate Formation marker beds can investigate areas for faulting. The PFS faulting can explain variations in highly correlative Westgate Formation bedding, as evident in the well control. The faulting can be explained by high-silica content densification and subsequent glass transition of siliceous strata; this includes high-silica content biogenic strata. Alternatively, the alteration of bentonite beds within the Westgate Formation strata could explain bed dissolution with subsequent polygonal faulting initiated. Finally, the polygonal faulting may affect Westgate Formation properties and shallower bed permeability.

Geologic framework

Beneath the expanse of the Great Plains lie sediments deposited in the Cretaceous WIS (see Fig. 1). The WIS was a large inland sea that spanned across North America from the Tethyan Sea in the Gulf of Mexico north to the Arctic Sea from the mid-Cretaceous to the early Paleogene (Catuneanu et al. 2000). The WIS split the North American continent into two land masses—Laramidia to the west and Appalachia to the east. The WIS hosts a succession of sediments, including a

Fig. 3. Four logs from a portion of the 2-25-17-16W3 wellbore. The BFS (Base of Fish Scales marker at the base of the Cenomanian) and Westgate tops are correlated to Prokoph and Atgerberg (1999), Pedersen (2004), and Schröder-Adams et al. (1996). The range of depths for faulted Westgate strata is shown. 2WS, Second White Specks. Zourob (2020) examined Westgate Formation parasequences west of the Success area.

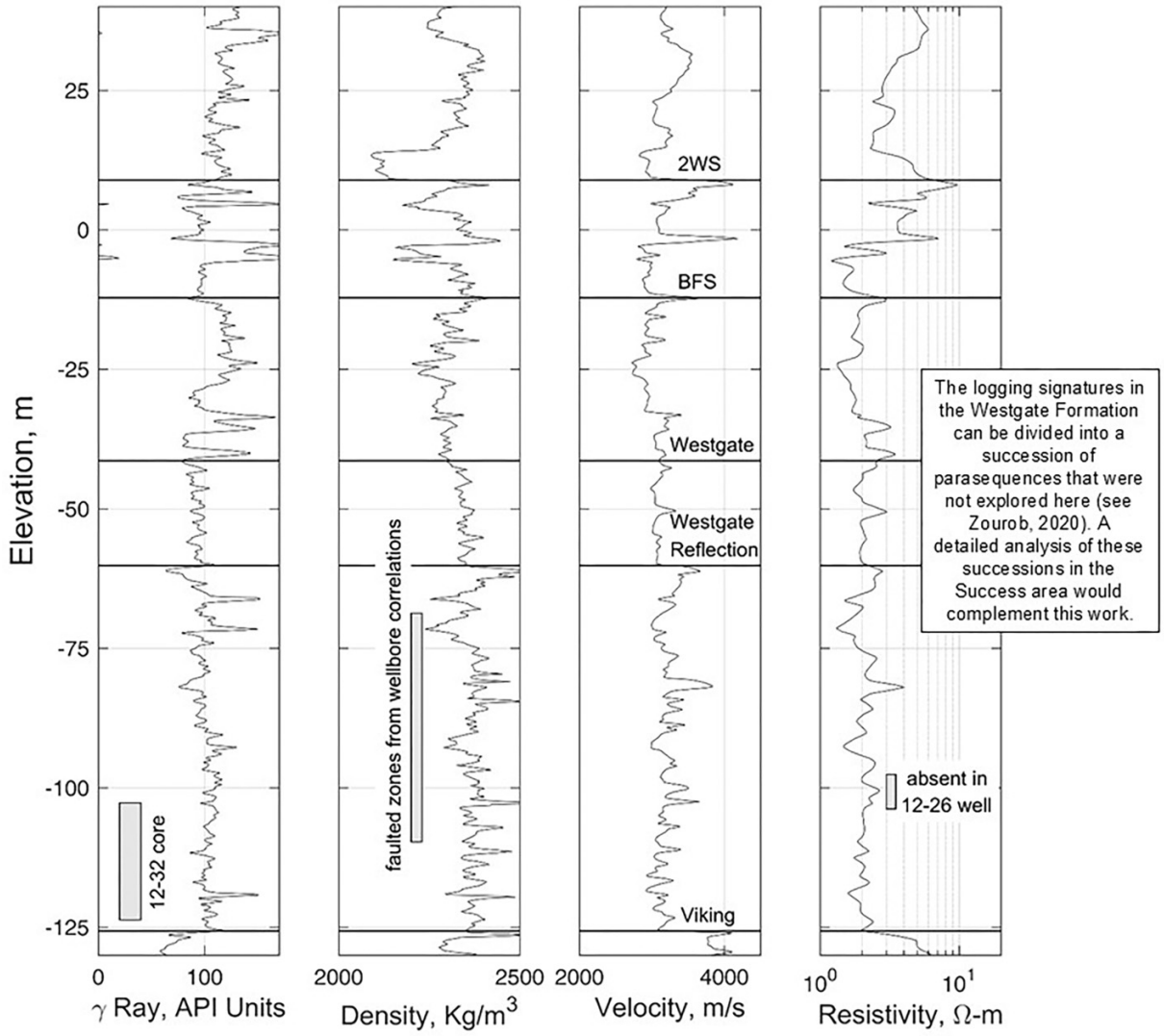

large volume of continental muds and clays (see Schultz et al. 1980; Roberts and Kirschbaum 1995, for example), bentonite, and other fine-grained material (Leckie et al. 2000).

Westgate formation

The Late Albian Westgate Formation comprises medium grey, noncalcareous marine shales interbedded with minor amounts of thin siltstones (McNeil and Caldwell 1981). The Westgate Formation was defined by McNeil and Caldwell (1981), with the type locality at National Hills, Manitoba (Fig. 1). The Westgate Formation was deposited during the initial stage of the Mowry Sea transgression as the WIS formed across North America (Leckie et al. 2000; Fig. 1). The marine transgression occurred over most of the Great Plains of North America from late Albian to early Turonian time (Williams and Stelck 1975). Bloch et al. (1999) describe the Westgate Formation as a progradational siltstone to mudstone deposited above storm wave base in the Mowry Sea. The Westgate Formation is part of the Lower Colorado Group (Table 1), with lithostratigraphic formations that can be mapped in the subsurface across western Canada (Bloch et al. 1993).

The Westgate Formation is thought to lie conformably on the Viking Formation (Caldwell and North 1984; Caldwell et al. 1993) and be subsequently overlain unconformably by the Fish Scales Formation (Pedersen et al. 2001) and the Turonian Second White Specks Formation (2WS). The 2WS lithology provides a consistent seismic reflection maker throughout western Canada. The Westgate Formation was deposited over ~1.5 Ma between ~98.7 and 97.2 Ma (Schröder-Adams et al. 1996). The Westgate Formation is the homotaxial equivalent of the Mowry Shale and the Shell Creek Shale in the northern United States (McNeil and Caldwell 1981).

Published maps showing the isopach of the Westgate Formation are scant. The Westgate Formation and homotaxial

Fig. 4. An explanation for the calculation of correlation throw curves used in this study. In this image, two resistivity logs from the Marie Lake, Alberta, area show faulted zones. A comparison of the stratigraphic elevations correlated between the wellbores defines the correlation throw curves. Three curves from the Success area show early and late faulting. 2WS, Second White Specks.

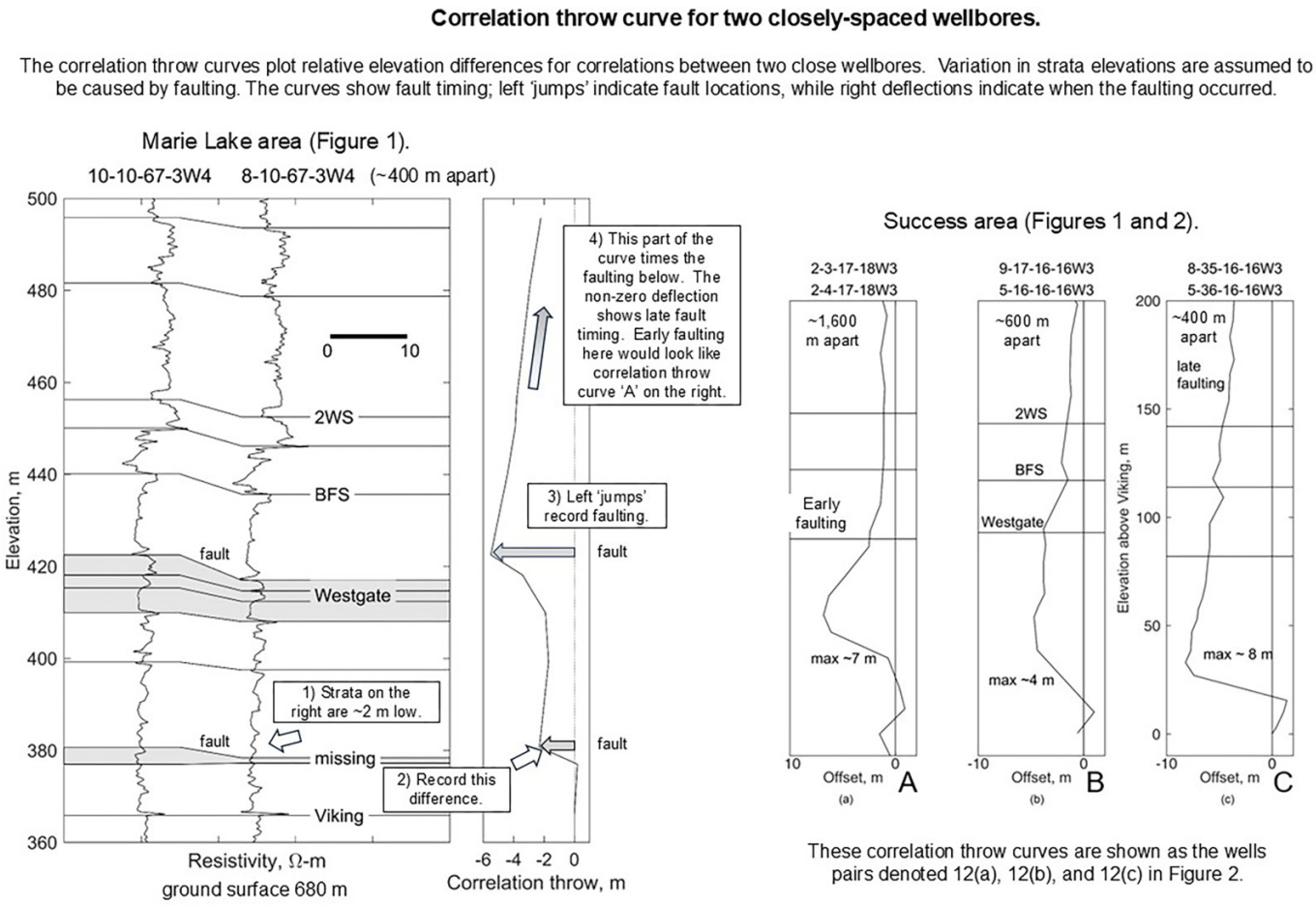

equivalents were believed to be deposited in lows in the Tethyan Sea that could vary in thickness throughout the WIS. Figure 1 shows an inset of a Westgate Formation isopach map based on the Williston Basin Targeted Geoscience Initiative between academia and governments (TGI Williston Basin Working Group 2008). The isopach values in western Saskatchewan and eastern Alberta are consistent with this map.

Mowry Shale

The Mowry Shale in the USA is homotaxially equivalent to the Westgate Shale. The Mowry Shale descriptions are consistent with Westgate Shale descriptions. For example, Longman et al. (2019) describe the Mowry Shale as below storm wave base deposits of dark grey, very fine-grained shales, typically containing less than 30% detrital clay by weight and over 50% quartz, sometimes locally up to 80% quartz. The quartz is described as a mix of biogenic grains, mainly radiolarians and authigenic silica, along with some detrital quartz silt of extrabasinal origin (Longman et al. 2019). The Mowry Shale has abundant fish scales and radiolarian tests and is interbedded with bentonite and sandstone layers (French et al. 2022). Many bentonite beds have been identified throughout the Mowry Shale interval across the Wind River Basin, Wyoming; these are thought to have been sourced from volcanoes to the west (Finn 2021). Finally, Milliken and Olson (2017) noted illite–smectite (I–S) beds in 46% of the clay mineral fractions of samples from five wellbores in the prevalence of quartz and other clay minerals in the Mowry Shale in the Rocky Mountain region.

Canadian study areas

The Westgate Formation has been logged in thousands of wellbores around the village of Success, Saskatchewan (Fig. 2). Most of the almost 2800 wellbores shown were drilled for deeper pool targets. Production from the area is from deeper Cretaceous and Jurassic reservoirs, where oil production was discovered in 1953. The underlying Viking Formation sandstone is productive ~30 km northwest of this area. Companies have cored the Viking zone in some wellbores, sometimes coring the overlying Westgate Formation. Several wellbores have core descriptions, such as at "11-16 core" (Fig. 2), where ~30 m of Westgate Formation core has been described and analyzed, ~4 km away from one of the 3D seis-

Fig. 5. Westgate zone interpreted seismic reflection two-way traveltime map. The stratigraphic depth for the corresponding impedance contrast is shown in Fig. 3. The grabens in the blue and purple areas are travel times lows corresponding to faulting at the Westgate level.

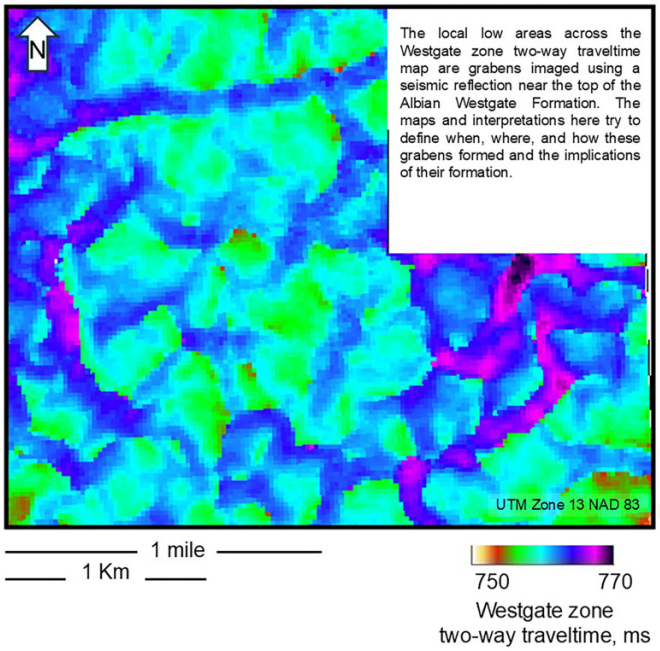

mic datasets used in this analysis. The core is predominately very fine to fine iron-stained siltstone with many vertical fractures. The porosity averages 22%, and the grain density averages 2620 kg/m^3. Permeabilities range from 0.5 to 1000 mD, with measured vertical permeabilities of up to 373 mD.

Figure 3 shows portions of four wellbore logs from the 2-25-17-16W3 wellbore (Fig. 2). This wellbore is within the bounds of the Success 3D seismic data presented here, but its precise position has not been identified on the confidential dataset.

Core descriptions corroborate many other observations of the Westgate Formation. For example, at Stony Plains in northern Alberta (Fig. 1), an outcrop of the Westgate Formation has been described as dark grey to black, organic-rich, noncalcareous, finely laminated mudstone that has a blocky fracture on weathered surfaces (Hay et al. 2012). At this outcrop, the lower 5 m of the Westgate Formation is not exposed due to slumping. Sulfur staining is commonly observed along fractures, and cone-in-cone calcite structures were also observed.

Southeast of the Stony Plains outcrop, the Westgate Formation is at a depth of ~250 m. Here, the zone is also cored in several wells. For example, at 10-10-67-3W4, an 18 m core encountered predominantly shaly siltstone. The logging suite from this well is compared to another wellbore (~400 m apart) to produce a correlation throw curve. The relative differences in the elevations of correlative beds produce the curve. This curve shows when the faulting occurred in time, as explained in Fig. 4. There are two stages of faulting within the Westgate Formation at Stony Plains: an early stage removed ~2.3 m of section, and a later stage removed ~4 m of section. Unlike the Success area (see the curves on the right side of Fig. 4), faulting occurs near the top of the Westgate Formation shale in the Marie Lake, Alberta area. These correlation curves exemplify typical faulting start, maximum fault throws, and fault timing variations observed in this analysis. All observed faulted zones occur within a range of depths within the Westgate Formation, as shown in Fig. 3. The earliest faulted Westgate Formation zone is ~15 m above the top of the Viking.

Wong et al. (2011) examined casing integrity in strata undergoing steam injection in Cold Lake, Alberta (~25 km south of Marie Lake in Fig. 1). They also noted the lithology of the Westgate Shale Formation. The Westgate Formation is characteristically heterolithic, comprising dark, finely interbedded siltstone, shale laminae, and minor bentonite layers. The authigenic silicate minerals in the Westgate Formation include quartz, I–S, kaolinite, and glauconite. Pyrite is also abundantly present in the shale.

At Dollard, Saskatchewan, the Westgate Formation was examined in 139 wellbores for this study (Fig. 1). Seismic data were not evaluated in this area. However, 50 vertical wells had lithological descriptions for the Westgate Formation strata. These descriptions are available from provincial government databases that can be accessed with software such as Accumap, which is used as a primary information aid for hydrocarbon exploration. The lithological descriptions for strata encountered in three wellbores (their locations are shown in Fig. 1) are very consistent. The zone is described as light to medium grey shale, slightly calcitic, with fossil debris and a very fine texture; it is a subfissile to fissile and blocky, very fine siltstone. As discussed below, the wellbores were used to compute the Westgate to Viking isopachs for the area.

Seismic data

The 3D seismic datasets for this work comprise two data volumes totaling 42.2 km^2, acquired at confidential areas in the Greater Success area (at Success and Leinan, see Fig. 2). An interpretation of the Success 3D seismic dataset is presented here. There were 110 wells drilled through the Viking Formation within the bounds of the datasets. The datasets were acquired to image deeper oil and gas targets within the Lower Cretaceous and Jurassic sediments ranging from ~950 to 1000 m deep. The seismic data were recorded using vertical component geophones and either dynamite or Vibroseis sources and were processed to enhance the P-wave energy signal-to-noise ratio. The data were processed to final stacked datasets, and post-stack time migrations were applied.

The data fold in the zone of interest was ~10 for all data. The data had interpretable signals up to 100 Hz based on frequency panels. Minor amounts of acquisition footprint (−20 dB compared to peak signal reflection amplitudes) were apparent on the data down to the Viking reflection. The data phase was deterministically estimated by matching stretched sonic and bulk density logs to construct a least squares wavelet estimate at the well tie points. The phase was rotated to display a positive impedance contrast (i.e., low to high velocity with increasing depth) as a peak, zero-phase reflection.

Fig. 6. Westgate seismic marker to Viking isochron versus isopach crossplot using the Success area 3D seismic data and the 29 wellbores from within the bounds of the survey.

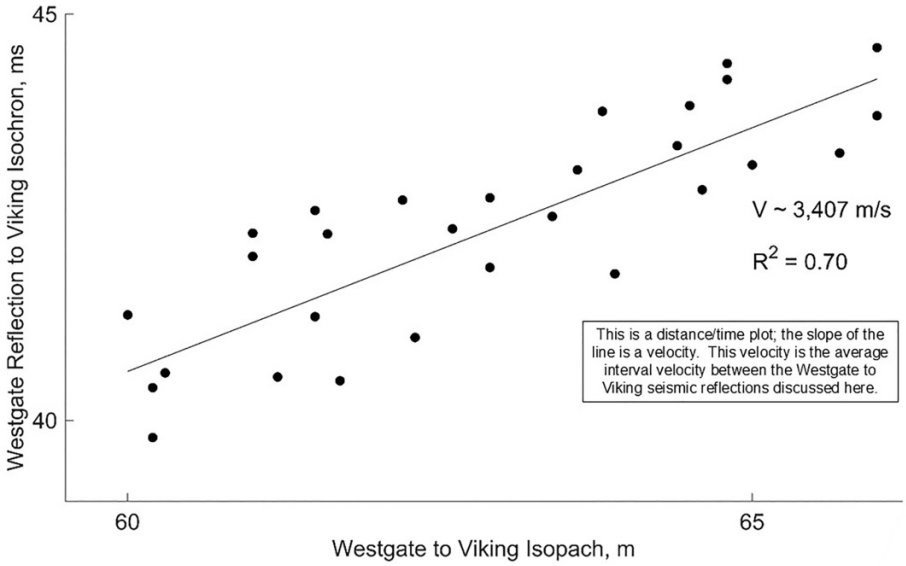

Fig. 7. Westgate seismic marker to Viking isopach computed using the velocity shown in Fig. 6. The average graben width and depth are ~125 and ~10 m, respectively. The locations for all the seismic line displays are shown here.

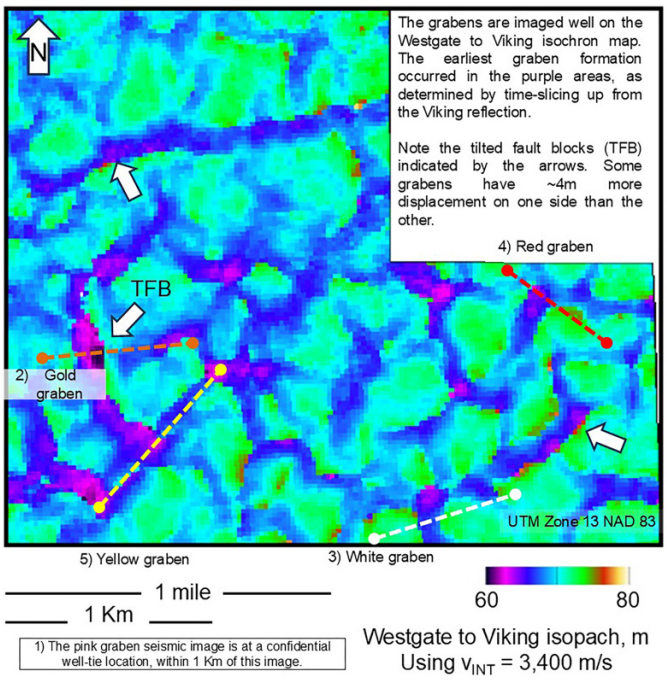

Observations and data interpretation

There are many seismic maps presented here. The seismic data are introduced, and then the rationale of the seismic mapping is presented. The mapping presented here tries to locate graben edges or time the graben formation. Figure 5 shows the Westgate seismic marker to the Viking isochron from a TGS dataset at Success, Sask. The reflections were interpreted by comparing sonic logs from four wellbores within the bounds of the dataset to rotate the data to zero phase, as discussed later. Geological tops from the wellbore were used to determine corresponding seismic data reflection horizons. The Westgate to Viking isopachs from 29 wellbores within the bounds of the Success 3D dataset were compared to the corresponding isochron values for the 3D seismic data. The crossplot is shown in Fig. 6. The slope of the least squares of this line is ~3400 m/s. This velocity was used to convert the isochron values from the seismic dataset to the isopach values shown in Fig. 7. Variations in the Westgate Formation seismic event are assumed to cause these isochron and isopach variations. The Viking seismic reflection is a conformable deeper contact, with no apparent sharp variations within the seismic dataset.

Some simple statistics were estimated from inspection of the grabens shown on Westgate two-way traveltime isochron (Fig. 5). The lengths and directions for 60 grabens were estimated (Fig. 8). The mean graben length was 380 m, with a mode length of 336 m in random strike directions. The graben lengths ranged from less than 200 m to almost 800 m. The strike of the grabens is random. Also shown are Westgate to Viking isopachs from the study areas. The isopach intervals calculated using wellbore information or seismic isochron values have a modal isopach distribution. This distribution is indicative but not a definitive determination of PFS in the Westgate Formation.

The most remarkable features on the isopach map (Fig. 7) are the grabens that are pronounced thins in the isopach value (blue- and purple-colored areas). The grabens only have 3–10 ms of negative relief and are imaged well on the seismic reflection entitled "Westgate Formation". Figures 9 and 10 are two seismic lines extracted across the dataset to exemplify the data. Both seismic lines are flattened and unflattened at the Viking; this is a regional datum here. These seismic data

Fig. 8. Histograms showing (*a*) graben strike length and (*b*) graben strike direction for 60 graben edges observed in Fig. 5. The graben lengths were estimated by inspection. The graben lengths appear to be determined by the free distance along strike until they encounter another graben. The images (*c*) to (*f*) are Westgate to Viking isopachs from the three study areas and the Success 3D seismic data estimates.

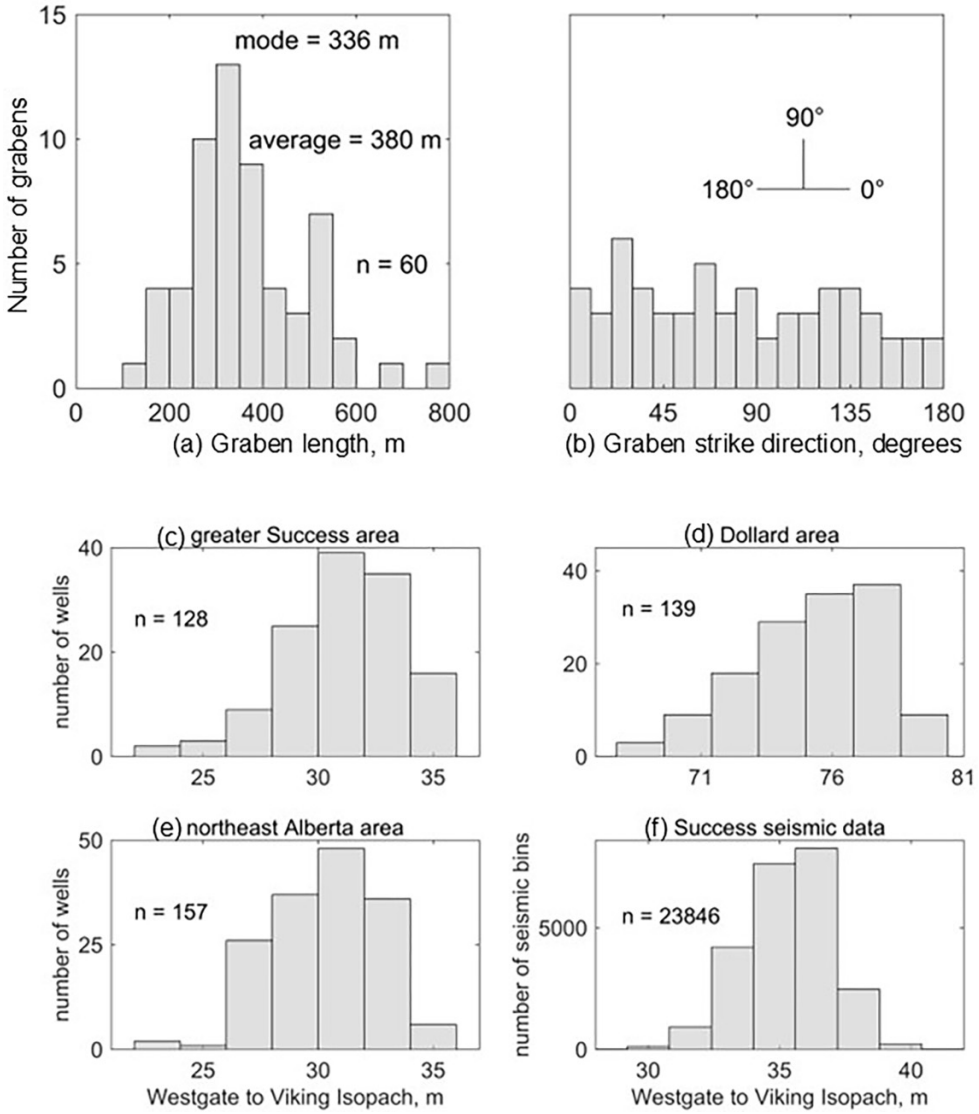

show five strong seismic reflections analyzed using various maps. The seismic data reflections and pertinent comments about each are below; consider Figs. 9 and 10:

- Niobrara—The Niobrara seismic reflection is a negative impedance contrast, implying a high- to low-velocity change on these zero-phase data. Many shallower reflections were interpreted on the seismic data. The Niobrara reflection is the shallowest seismic reflection that images effects of the grabens discussed here. The strata above this reflection are unconformable to the strata examined here.
- Carlile Zone—This peak seismic reflection was interpreted because of its lateral consistency. Isochron maps using this reflection and the adjacent reflections above and below show subtle, consistently thick areas across the grabens during the time intervals examined using this reflection.
- 2WS—The positive impedance contrast for the Turonian Second White Speckled Shale zone is at the interpreted peak reflection, "Turonian 2WS". This contrast occurs throughout the WIS. Some variations in this traveltime are attributed to the dissolution of deeper Westgate Formation strata.
- Westgate—The Westgate seismic trough reflection is from an impedance contrast at the elevation shown in Fig. 3. This seismic data reflection is relatively weak in amplitude but consistent, and it is the only seismic event to show conspicuous faulting and the obvious grabens.
- Viking—The Viking peak seismic reflection is a high-amplitude, consistent peak across the dataset. It is assumed that the Viking seismic reflection can be used as a datum for the calculated Westgate to Viking seismic reflection isopach (Fig. 8). The strata below this reflection are unconformable to the strata examined here.

Fig. 9. The southwest-to-northeast seismic line is located in Fig. 7. Isochron maps for each of the four zones and regional/residual estimates of these maps are presented here. Note the faulting at the Westgate reflection. Maps highlighting the faulting offset and amplitude variations in the Westgate seismic reflection amplitude are discussed here. 2WS, Second White Specks.

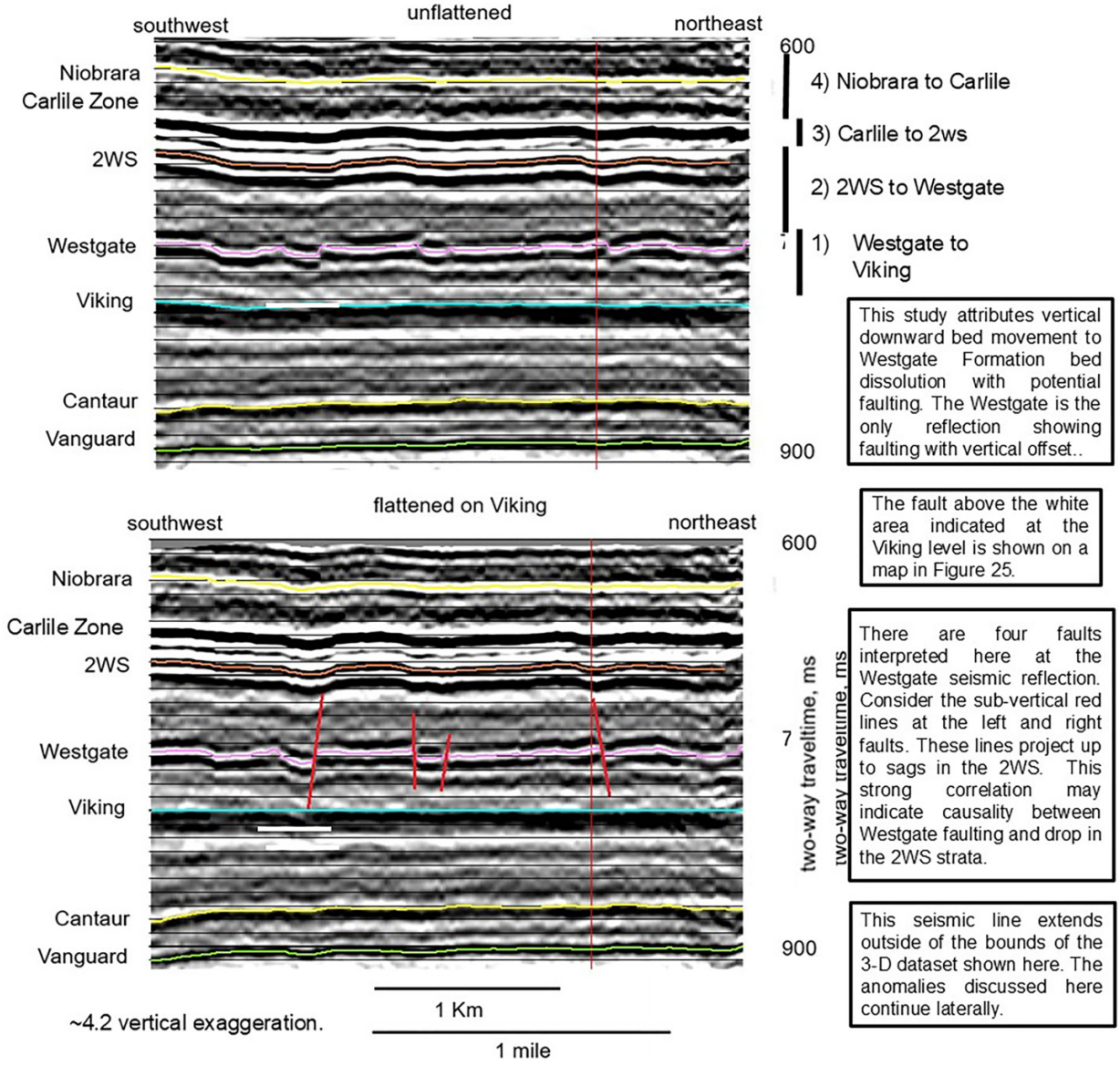

There are minor temporal variations on the 2WS traveltime across both seismic data displays in Figs. 9 and 10. Also, a preliminary interpretation of the correlation throw curves led to the belief that some areas of the shallower 2WS surface might have been affected by late faulting. The Turonian 2WS two-way traveltime map was residualized, as described in Fig. 11 and shown on the maps displayed in Figs. 12–14. Note the sonic log from a wellbore and how it compares to the seismic data (Fig. 11). A synthetic seismic trace is shown next to the seismic data. This trace was calculated by using the sonic log to compute reflection coefficients. These were convolved with a 10/15-75/90 Hz, zero-phase Butterworth wavelet to produce the synthetic seismic trace.

Understanding how the residual maps were made for the displays shown here is essential to this work, as there are many. Least-square estimates of polynomials from a planar surface to a seventh order were fitted to the two-way traveltime and isochron (time-difference) maps within the bounds of the 3D seismic survey. These maps were visually inspected for the lowest-order polynomial map that constructed a balanced residual map. All maps are presented here or in the supplementary images for completion. Figure 12 shows the Turonian 2WS two-way traveltime map. There are two purple areas on the northwest and east sides of Fig. 12. Fitting a sixth-order polynomial to these data preserves these low areas in Fig. 13, as the higher-order polynomials can fit maps with curvature, like the data in Fig. 13. When this map is subtracted from the map in Fig. 12, the residual map in Fig. 14 is produced. The residual map shows values balanced in colors (and values) across the map sheet. The residuals on this map

Fig. 10. The northwest-to-southeast seismic line is located in Fig. 7. This is a good image to note the undulating Turonian Second White Specks (2WS) and the faulted Westgate reflection on the flattened data at the bottom of the display.

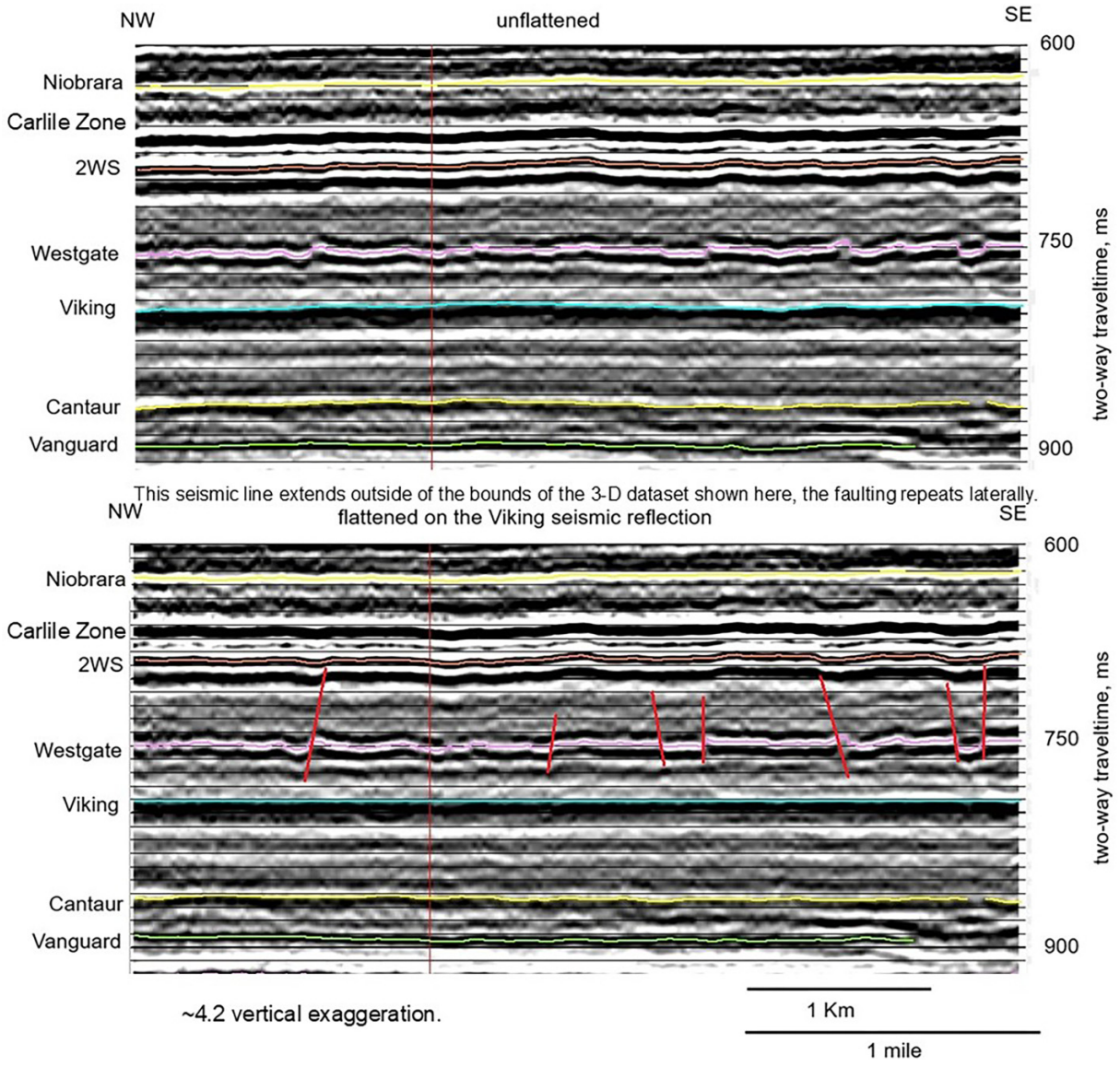

have a mottled look, like Fig. 12. These red negative residuals in Fig. 14 were used to construct the yellow outlined areas on the map. These areas are plotted on other maps here. It is believed these areas represent post-Turonian 2WS graben formation, causing downward movement on the shallower strata.

Some Westgate faults are evident in these seismic data. These faults are interpreted on the flattened seismic data sections at the bottom of Figs. 9 and 10. However, fault traces for the grabens were not interpreted on the seismic datasets. The large number of faults imaged at the horizon would make fault trace interpretation time-consuming and difficult for dip estimation. Instead, as discussed below, the faults were located with seismic reflection amplitude interpretations and mathematical analyses. Figure 15 shows a summary of the Westgate seismic reflection amplitude maps that are shown here. The Westgate seismic reflection amplitude (Fig. 16) and the computed gradient map (Fig. 17) are preferred in this analysis, as discussed below. Figures S-1 (edge-detection diagonal down) and S-2 (maximum curvature) show two more maps highlighting fault edges.

The computed gradient maps for the Westgate Formation faults (Fig. 17) and flexures in the Turonian 2WS reflection (Fig. 18) were computed. Figure 19 shows areas of quick changes in the Westgate to Viking isochron correlated to high seismic reflection gradient areas. Figure 20 shows areas where the high-values gradient areas for the Westgate and the 2WS seismic reflection gradients pair; many areas are identified. These pairings imply a relationship between the Turonian 2WS seismic reflection flexures and faults in the Westgate Formation. This relationship estimates bed movement at ~30° dip, as explained in Fig. 20.

The 3D seismic dataset at Success, Saskatchewan, maps four intervals. Consider the top of Fig. 9; these four inter-

Fig. 11. A discussion regarding the Turonian Second White Speckled Shale (Second White Specks (2WS)) two-way traveltime and corresponding regional/residual map estimations. Residualization was done for all studied isochrons as well. The Turonian 2WS is a seismic reflection that can occur throughout the WIS (McNeil and Caldwell 1981).

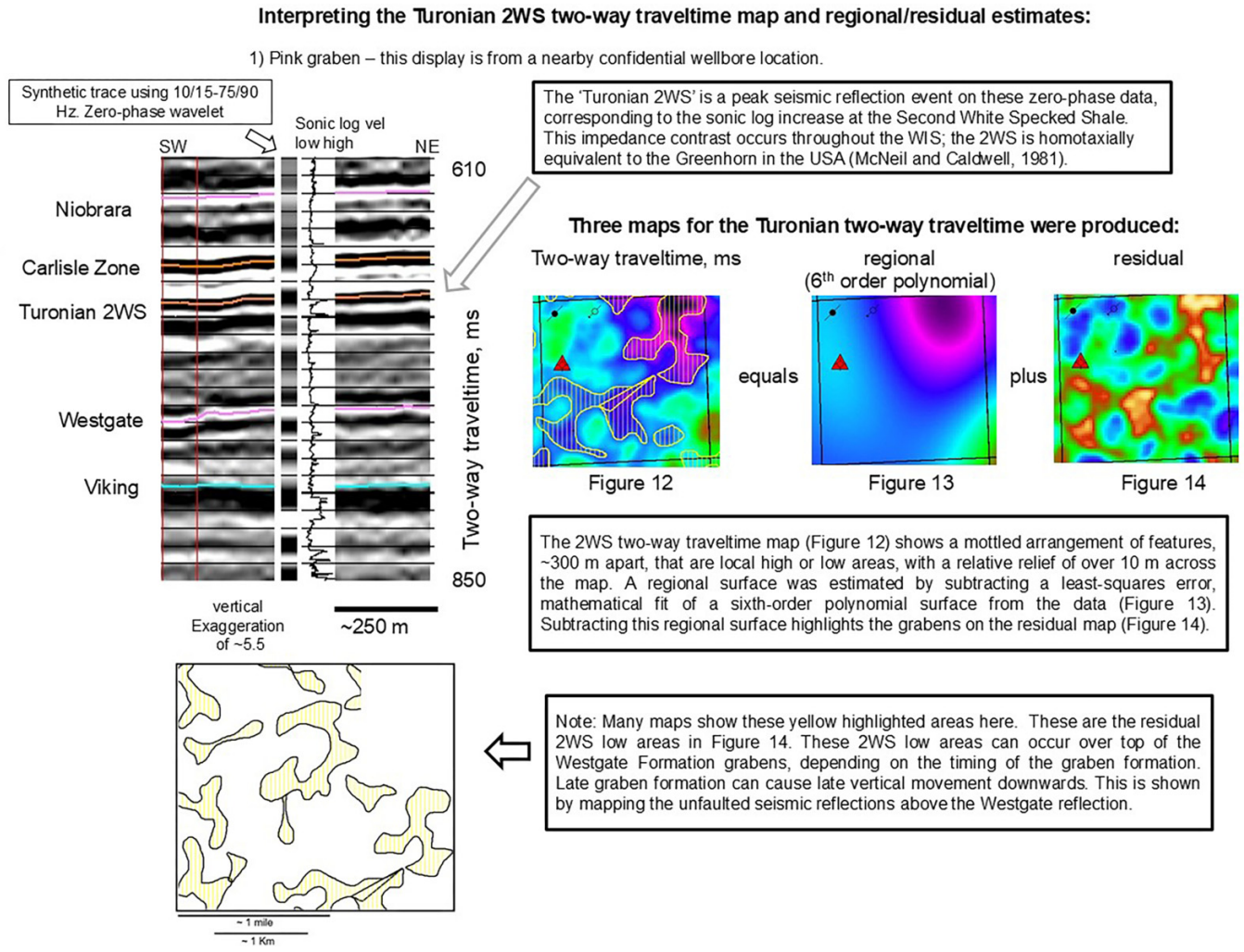

vals are shown. Five high signal-to-noise ratios and laterally consistent horizons were interpreted using the seismic data to produce the four isochron maps. As shown in Fig. 21, each of these four isochron maps were residualized by fitting a least-squares polynomial surface to the data. Figures 22–24 show maps for the shallowest isochron, the Niobrara to Carlile isochron. These images show the two-way traveltime, computed regional, and subsequent residual maps. The regional map is a simple second-order polynomial, least-squares fitted surface that strikes northwest to southeast. This map could represent a regional thickening in the southwest area of the dataset. The residual map shows faint features, represented by the green areas that occur over the same areas as the yellow areas that represent the residual 2WS low areas. These residual features are balanced in isochron value variations across the map. Similar residual maps for the Carlile to 2WS, the 2WS to the Westgate, and the Westgate to Viking are shown in Figs. 25–27, respectively (the original isochrons and regional maps for the three lower intervals are shown in Figs. S-3–S-8).

Discussion

Polygonal faulting

The plan view of the Westgate seismic marker to Viking isopach (Fig. 7) is presented as the primary evidence for the occurrence of a PFS. The image's blue and purple areas are considered grabens in the PFS. The image shows coalesced grabens that form polygons in plan view. The simple statistics in Fig. 8 show grabens edges measured with random strike directions. This randomness is usually observed by measuring faulting in PFS, not graben orientation. The Westgate PFS is hosted in fine-grained volcanogenic strata, consistent with other areas. This relationship is an important observation; volcanogenic strata's shear-thinning, rheological properties could be essential to PFS formation.

Actual faulting with displacement is limited to the Westgate seismic reflection in the data presented here. The seismic data contain three excellent seismic data reflections that have imaged negative movement over the grabens for up to ~20 MY. The maps presented here allow the reader to decide

Fig. 12. The Turonian Second White Specks (2WS) two-way traveltime. The areas shown in yellow are estimated residual lows on the 2WS two-way traveltime surface, as discussed in Figs. 13 and 14.

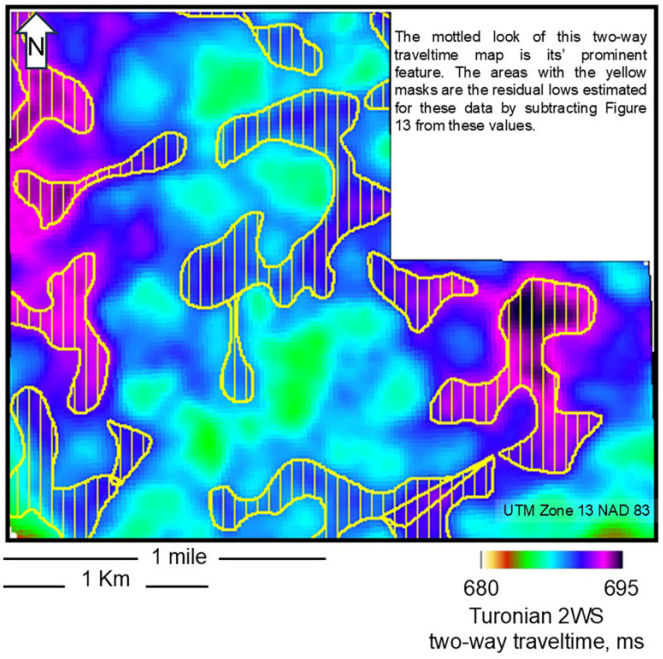

Fig. 13. A sixth-order polynomial map using the data represented in Fig. 12. The higher order polynomial is required to model the two circle areas on the map. 2WS, Second White Specks.

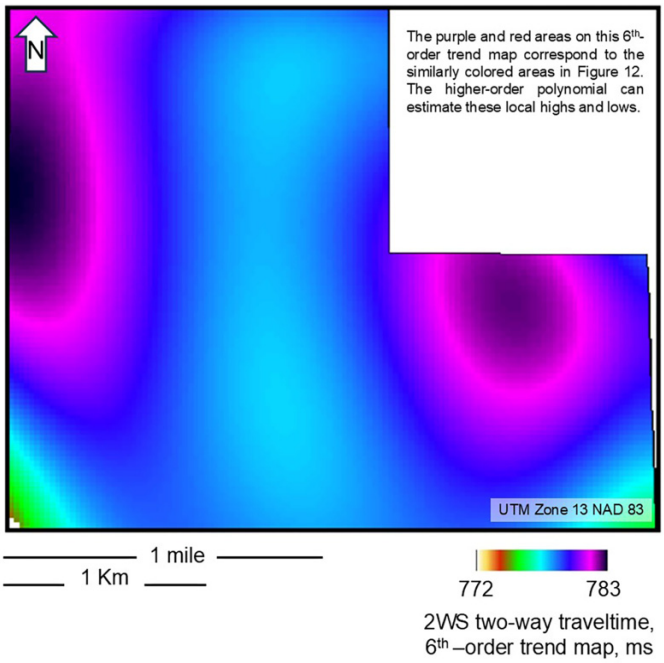

how features on each map relate to each other and how they correlate to the locations of the grabens presented here.

A few others present evidence of the Westgate Formation hosting polygonal faults. Zourob (2020) recognized polygonal faulting in Later Albian strata in an extensive review of northeastern Alberta. Polygonal faulting was recognized throughout the Westgate Formation in Alberta, using wellbore information from closely spaced well control. Zhang (2006) presented evidence of polygonal faults offsetting two levels within the Westgate alloformation. These zones correspond to the upper and lower Westgate Formation faulting observed at Marie, northeastern Alberta, as shown in Fig. 4. Zhang (2015) examined natural fracture systems in Mowry Shale outcrops (homotaxial to the Westgate Formation) in the Bighorn Basin, Wyoming. The outcrops showed faulting and fracturing at many angles, which was consistent with PFS formation. Many orthogonal fracture sets were identified but not as being hosted within a PFS.

Fig. 14. The Turonian Second White Specks (2WS) residual map was made by taking the difference between the maps shown in Figs. 12 and 13. The mottled red low residual areas define the yellow-shaded areas shown on many maps here. The occurrence of mottled areas on the Turonian 2WS in other areas may indicate the faulting shown here.

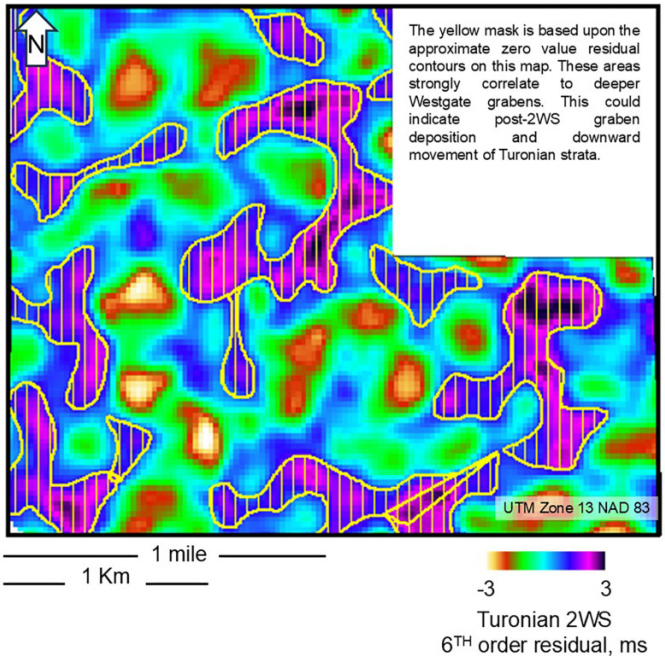

Seismic data interpretation

The observations using the seismic data presented here represent the two datasets analyzed in the Success area. A relatively low reflection amplitude P-wave arrival from within the Westgate Formation images structural variations defined by graben bounding faults. The reflection is subtle but can map details not observable in the well control. For example, wellbores "D" and "E" in Fig. 15 are only 325 m apart, but there is a complete graben between the two locations that is not encountered by either wellbore. Similar observations were made while interpreting the Upper Cretaceous Great Plains PFS in Campanian-aged strata (St-Onge 2017). Mapping with 3D seismic data consistently shows details not mapped with even closely spaced wellbores.

Fig. 15. A discussion regarding the Westgate Formation seismic reflection amplitudes. The process presented here was done for all amplitudes studied. 2WS, Second White Specks.

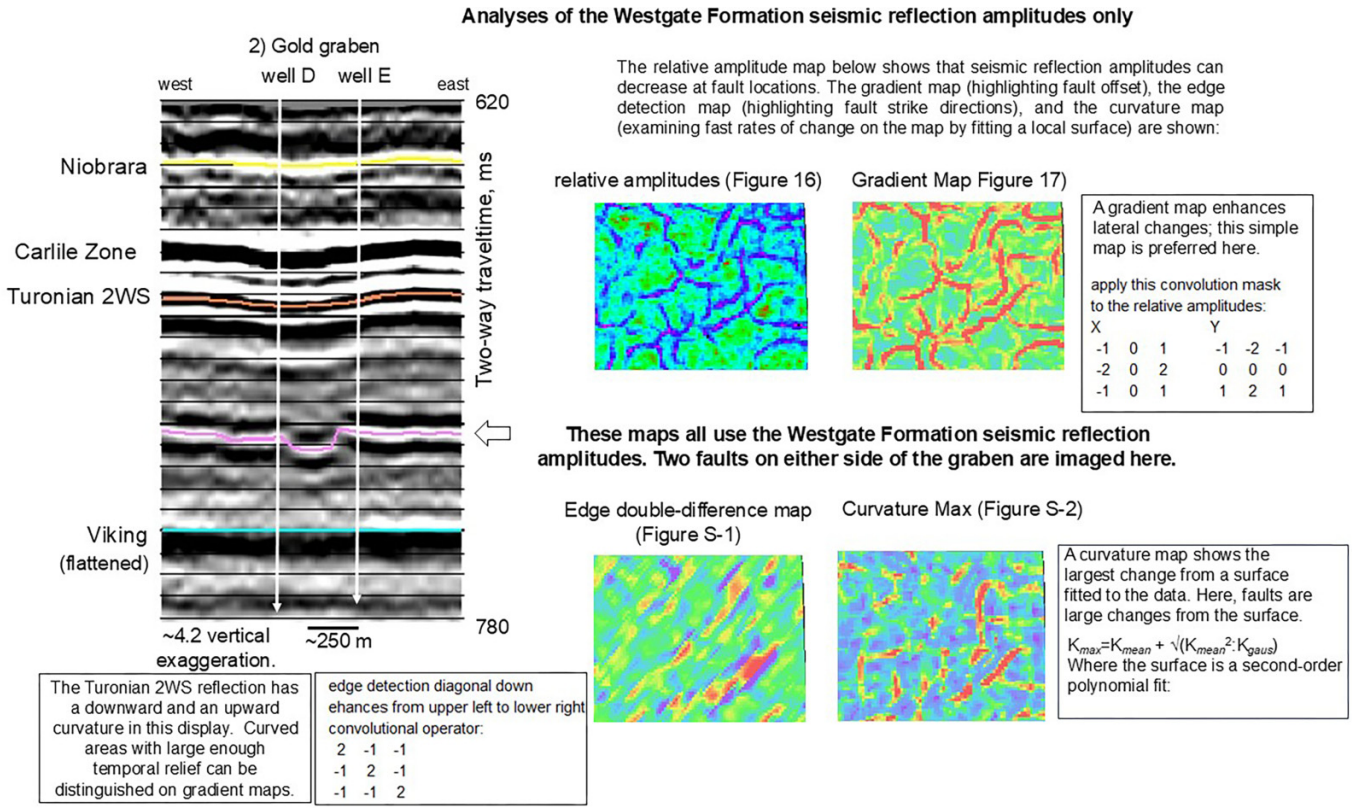

Fig. 16. Westgate seismic reflection amplitudes. The amplitudes decrease at fault edges.

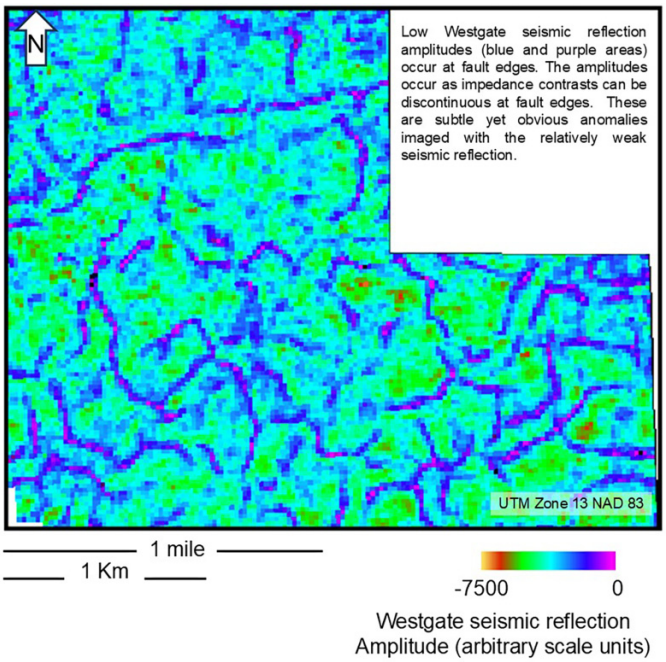

Fig. 17. Westgate seismic computed gradient. The gradients increase at the fault locations. The red areas are plotted in color in Fig. 19.

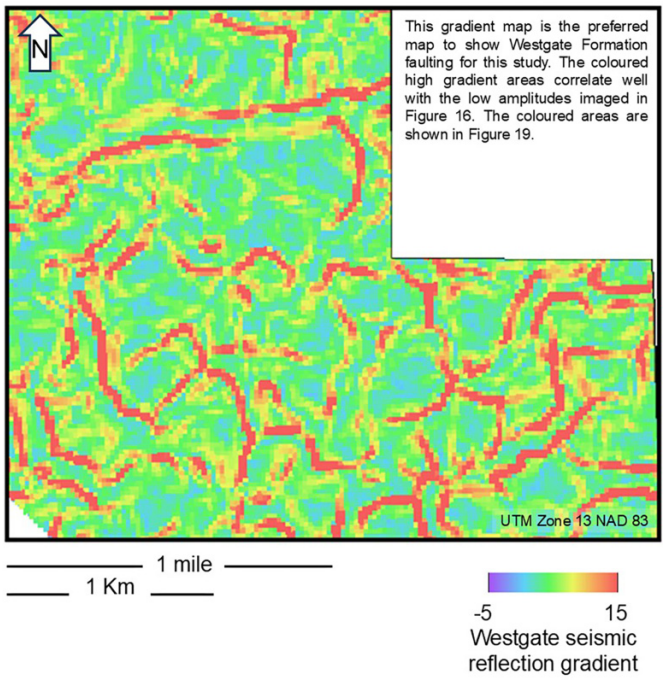

Fig. 18. Turonian Second White Specks (2WS) computed gradient. The gradients increase where the 2WS reflection quickly changes in traveltime but with no obvious faulted areas on the seismic reflection. The red areas are plotted on a greyscale in Fig. 20.

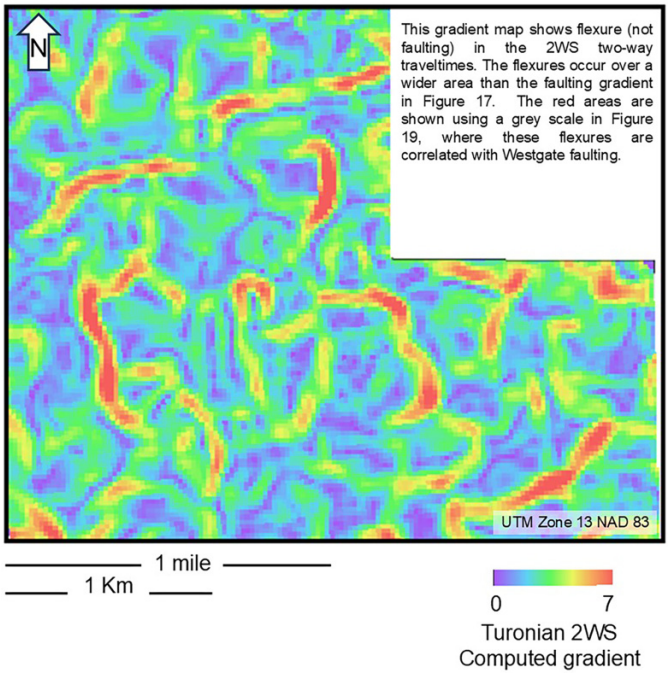

Fig. 19. A plot showing both the Westgate to Viking isochron values in greyscale along with colored areas showing high-value (>10) computed Westgate seismic reflection gradients from Fig. 17. The areas where the greyscale changes fast are also faulted areas, as indicated by the green to red coloring of the gradient values.

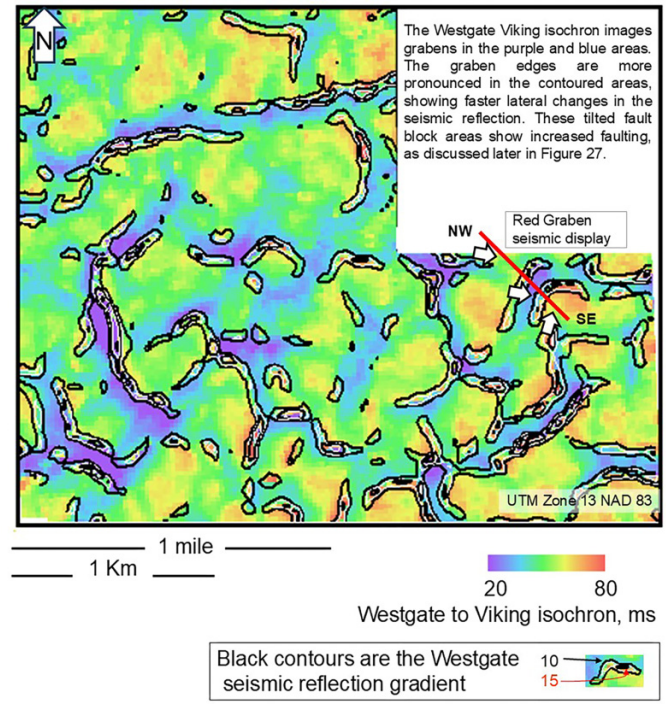

The grabens shown on the Westgate to Viking isopach (Fig. 7) were measured on both datasets. The measurements have statistics shown in Fig. 8: strike lengths up to 800 m for the grabens that are ~125 m wide and up to ~10 m deep. Most grabens are between 200 and 400 m long and end in both directions by intersecting other grabens. The average graben density for the two datasets is ~1.825 km of graben length/km^2 (the graben density value was estimated to compare results from the two seismic datasets). The graben spacing here is the same density as 125 m wide grabens spaced on center and 525 m apart in both directions. This occurrence shows pervasive polygonal faulting.

Faulting has occurred over a large area; the localities shown here total over 1000 km^2 and are ~600 km apart (Fig. 1). The PFS may continue between the two areas. An examination of an extensive seismic database throughout southern Saskatchewan showed that faulting does not occur in some areas, such as parts of eastern Saskatchewan. A simple mapping method that could also investigate the potential for PFS occurrence within the Westgate Formation and the homotaxial Mowry Shale in the United States is presented below.

The maximum observed fault throw is ~10 m, which appears relatively low compared to the PFS throws observed in other areas. For example, Watterson et al. (2000) observed faults in Australia's Lower Cretaceous Eromanga Basin with up to ~80 m of throw. Similarly, up to 80 m of throw has been observed in the Great Plains Upper Cretaceous Great Plains PFS (St-Onge 2017). However, these PFSs occur in sequences up to 1000 and 700 m thick, respectively. Expressed as a percentage of sediment thickness, the fault throws at Success (10%) are comparable to those observed in the Eromanga Basin (8%) and the Great Plains PFS (10%).

Polygonal fault timing determined using seismic data

The Westgate Formation PFS is layerbound, with most faulting occurring within these strata. Minor faulting (~2 m of offset) could be interpreted along the Turonian 2WS reflection in Fig. 9, but that subtle occurrence is only observed in three small areas. Examining the residual maps can help determine the timing of the Westgate Shale faults. Consider Fig. 21 again, showing snippets of the four residual maps. The uppermost map is a snippet of the data presented in Fig. 24; this is the residual of the Niobrara to Carlile. Consider the "regional" map in Fig. 23 used to make this residual. Again, this map represents regional thickening from northwest to southeast at this interval. When subtracted from the map in Fig. 22, this simple map shows residuals (Fig. 24) that correlate well with the yellow-shaded 2WS low areas. The green residual lows (~5 m of downward drop) occur across the 2WS lows and represent the late occurrence of Westgate faulting, captured between the age of the Niobrara and Carlile seismic reflection.

The Carlile to 2WS residual isochron is shown in Fig. 25. The residual lows in this interval are up to ~2 ms, which is ~2 m. These are very faint anomalies to be interpreted on seismic data acquired in the area; the imaging of these subtle anomalies attests to the high S:N ratio data. The faint anomalies correlate to the 2WS residual lows.

Fig. 20. A plot showing high-value gradient areas for the Turonian Second White Specks (2WS) and Westgate seismic reflections from Figs. 17 and 19, respectively. Six pairs are identified; there are more pairs in the image. These pairs show a correlation between vertical drops in the 2WS two-way traveltimes and Westgate Formation faults.

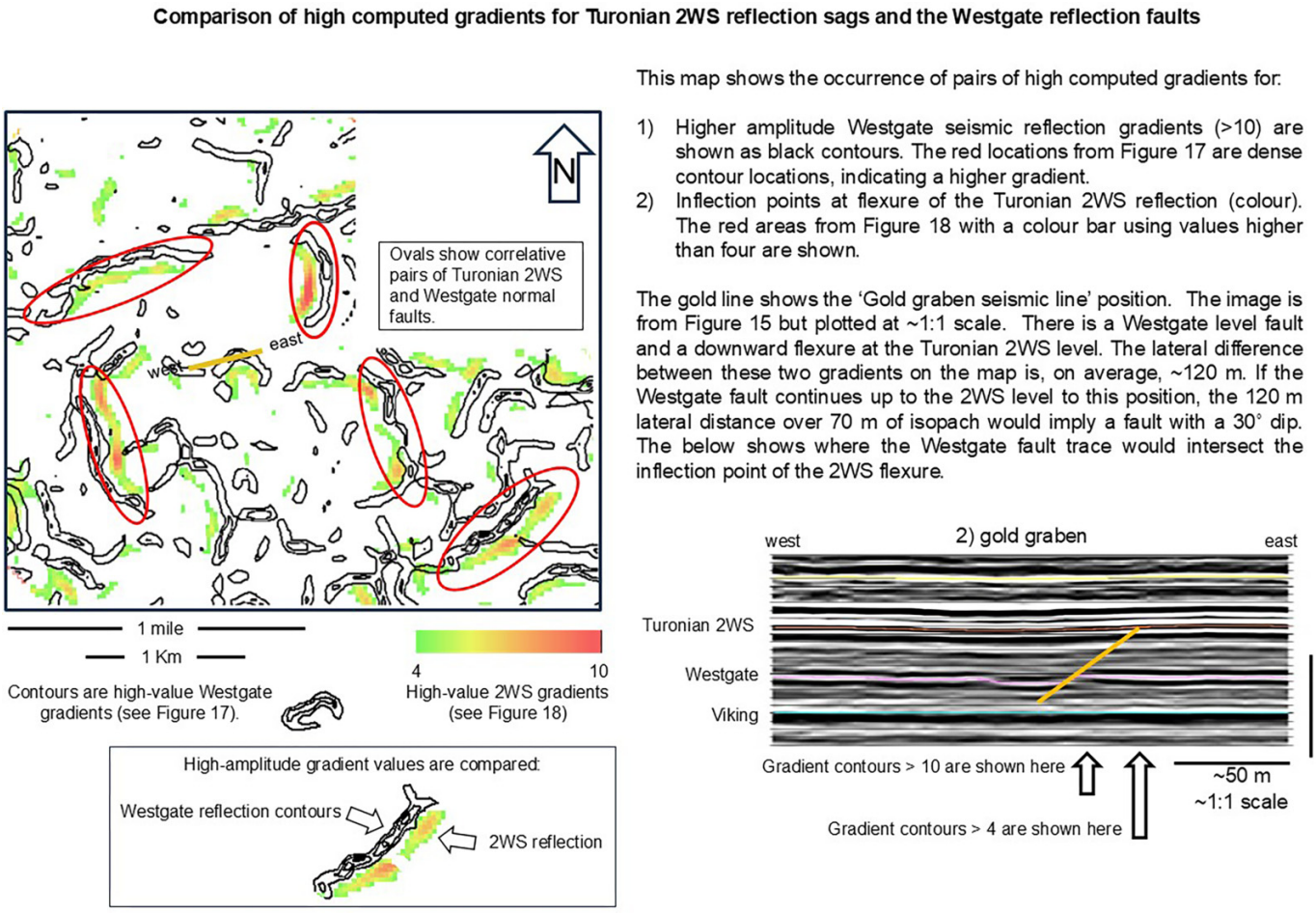

Figure 26 shows the residual of the 2WS to the Westgate isochron. The map is interesting; it shows many "pairs" of red and blue areas. Some of the map is caused by graben formation during this time interval. However, this time interval shows the effects of nonvertical faulting; this isochron is a bit more complicated to consider than the other isochrons because of the lateral offset of the 2WS flexures and the Westgate faulting (see Fig. 20). Consider the fault in Fig. 9 (and replotted in Fig. 20), above the white area on the Viking reflection. The sag in the 2WS seismic reflection is laterally displaced to the right of the fault trace at the Westgate formation level. This lateral difference occurs at ~30° dip. This angle might imply weakness along a natural angle of repose in the aqueously suspended strata (Al-Hashemi and Al-Amoudi 2018). The red and blue areas occur over the top of the 2WS residual low areas indicated in yellow on the map. This relationship should occur, if these variations are related to graben formation.

Figure 28 summarizes the timing of the graben dissolution examined here. Consider

- Up to ~10 m of downward movement in a subtle seismic reflection imaging PFS characteristics at the Westgate level.
- A continuance of graben later movement, as evidenced on the 2WS to Westgate isochron residual map, where up to ~5 m of dissolution continued at the graben edges.
- The Carlile to Turonian isochron residual map confirms faint (up to ~2 ms) downward movement during this time.
- The shallowest zone, the Niobrara to Carlile residual map, images wide residual areas (up to ~5 m drop) occurring over the 2WS residual lows.

All four intervals examined in this study show evidence for the timing of Westgate faulting. Figure 29 shows a crossplot that was done to check the residual mapping created here using the seismic data areochron values. The crossplot shows a good correlation between

- The estimated residual of the Westgate to Viking isochron (*x*-axis).
- The estimate of each residual map above the Westgate seismic reflection was added together (*y*-axis). Specifically, the residuals on maps in Figs. 24–26 were added together, point by point, on the seismic data grid.
- There is almost a 1:1 correlation on the crossplot; the sum of the calculated residuals is close in value to the residu-

Fig. 21. A discussion regarding the creation and analysis of four residual maps for the four intervals examined in this study. 2WS, Second White Specks.

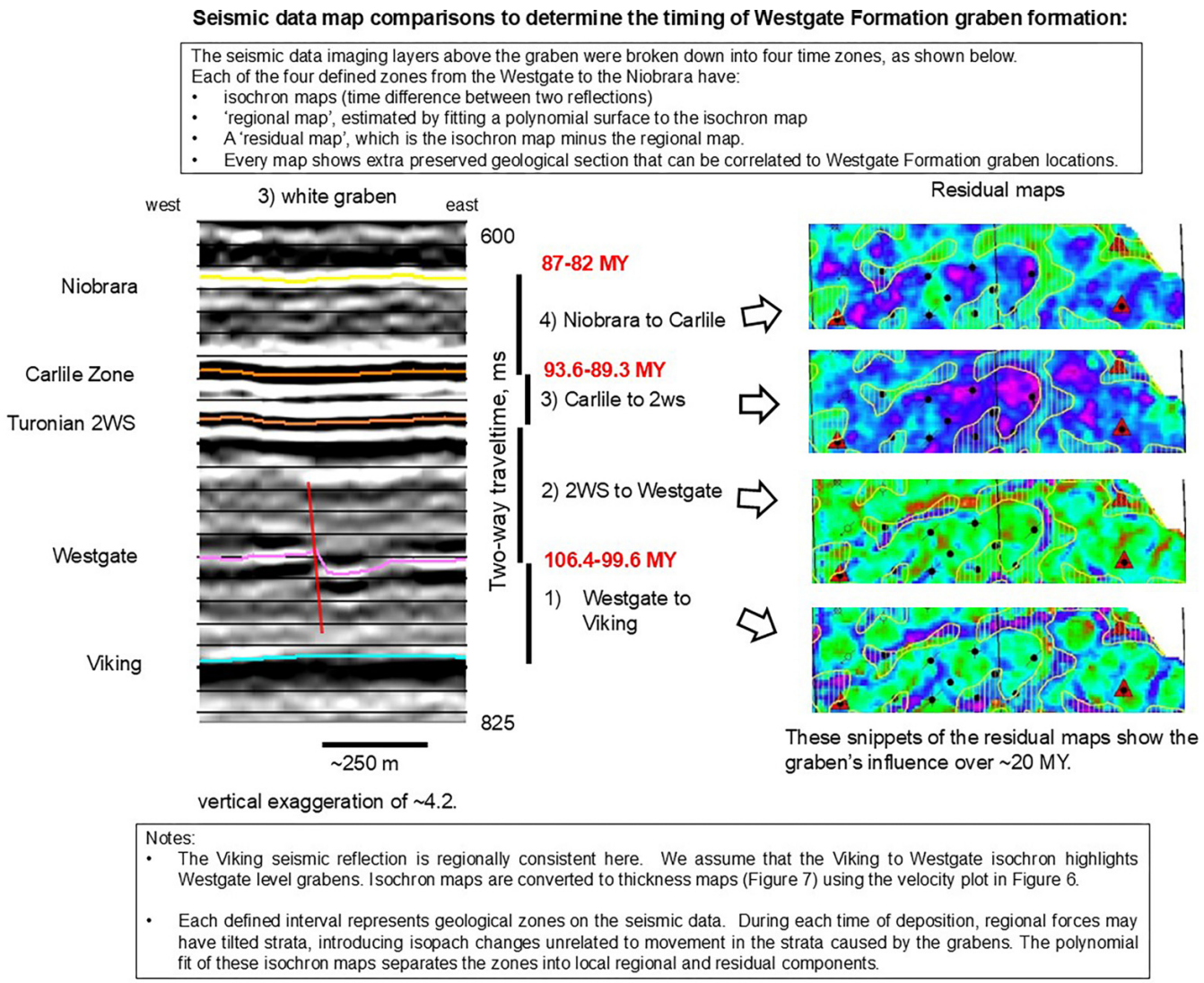

als that estimate the graben relief. Again, the upper three residuals are believed to map the timing of the Westgate Formation grabens, and about half of the movement takes place post-Turonian time. This crossplot provides evidence that the residual maps did not remove any effects of the graben formation. This observation should also be made clear by inspecting the regional maps.

Polygonal fault timing using wellbore data

Can the earliest fault timing for the Westgate Formation faulting be determined? To answer this, hundreds of wellbores were examined for this study. The Westgate Formation has missing section (as compared to adjacent wellbores) that varies from ~15 m above the Viking to the top of the Westgate Formation (see Figs. 3 and 4, for example). Schröder-Adams et al. (1996) date the Westgate Formation deposition to between ~98.7 and 97.2 Ma. At Success, the 2-25-17-16W3 wellbore has ~84 m of sediments (Fig. 3). These values correspond to a compacted sedimentation rate of 1 cm every ~180 years (almost 6 cm/10^3 years). This observation is consistent with Bloch et al. (1999), who estimated a range of sedimentation rates of 1–6 cm/10^3 years. If the lowest earliest PFS faulting is above 15 m of compacted sediment, this would imply PFS initiation in 15 m of compacted sediment ~180 000 years after the initial progradation of the Mowry Sea. This early timing of PFS initiation is consistent with observations by others (Cartwright 2011, for example).

Polygonal fault areal distribution

A simple measure that may help determine polygonal faulting within the Westgate Formation is the histogram distribution of a Westgate Formation marker to the Viking isopach or isochron (Fig. 8). All the histograms show a single-mode skewed distribution. The mode is weighted toward the unfaulted bed thickness. As the faulting occurs, the isopach values decrease. More faulting is observed (in the wellbores in an area or observed on seismic data) in the histogram cells

Fig. 22. The Niobrara to Carlile isochron. There is a mottled look in some areas of this map. Also, there is a dip from northeast to southwest.

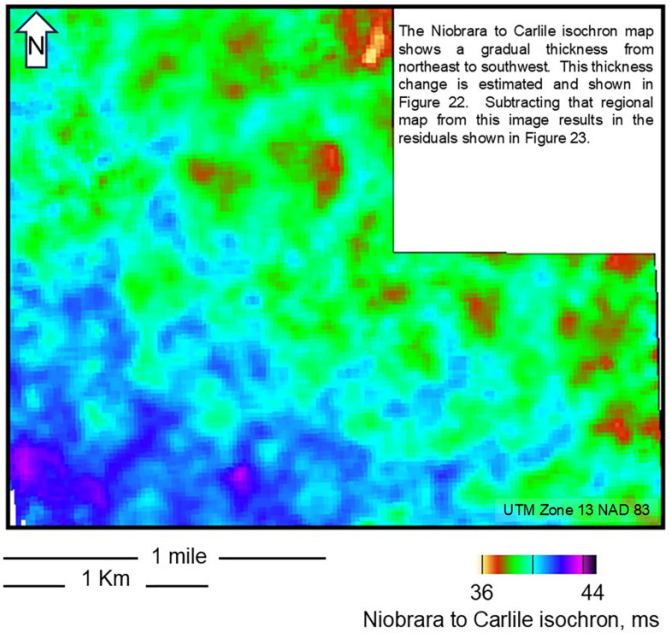

Fig. 23. A second-order polynomial fit to the data is shown in Fig. 22. This surface is defined as a regional trend for this interval. This trend corresponds well to the trend noted in Fig. 22.

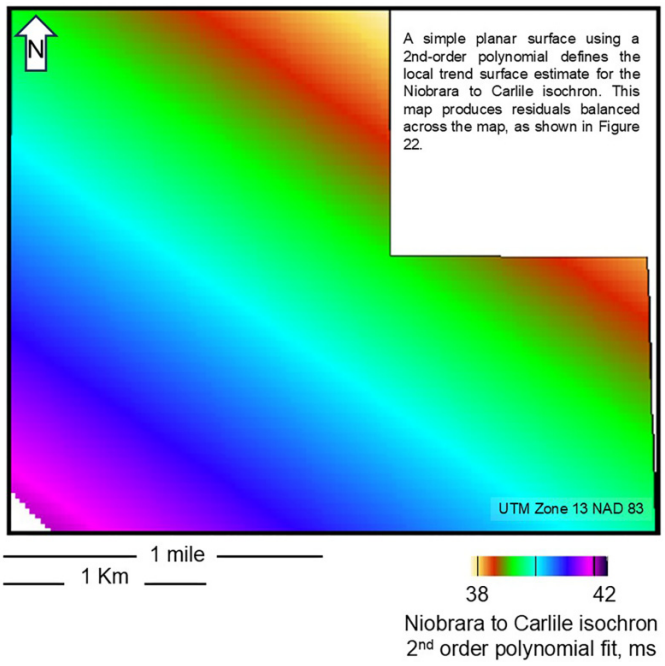

closest to the mode thickness. This pattern is observed in all study areas and on both seismic datasets in the Success, Saskatchewan area. Hopefully, this simple observation can help confirm Westgate Formation PFS faulting within its depositional bounds (Fig. 1). This analysis should be one char-

Fig. 24. The Niobrara to Carlile isochron shows faint but persistent residual lows that correspond well to the yellow-shaded areas defined by Second White Specks (2WS) residual low areas. It is interpreted that this correlation means the Niobrara to Carlile interval is thickening over the graben areas.

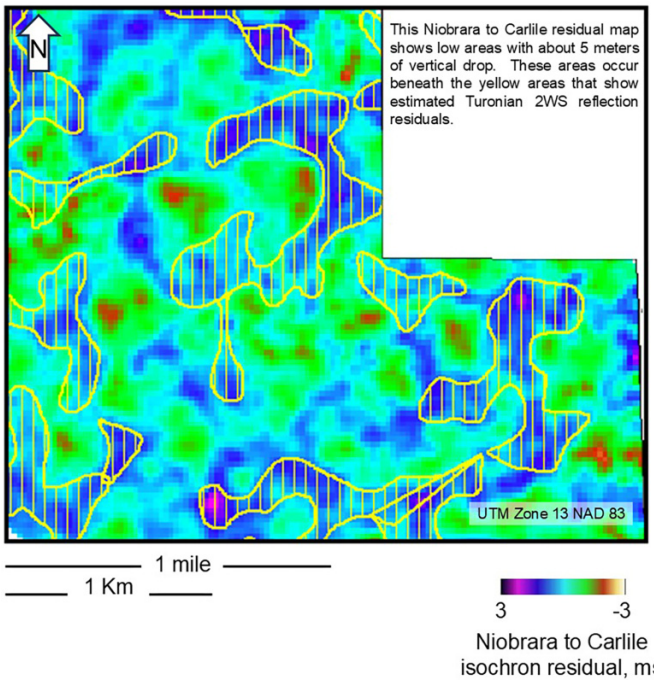

Fig. 25. The Carlile to Second White Specks (2WS) residual map was made by subtracting the data in Fig. S-3 from the data in Fig. S-4. Faint residuals for this interval correlate to the 2WS residual low areas.

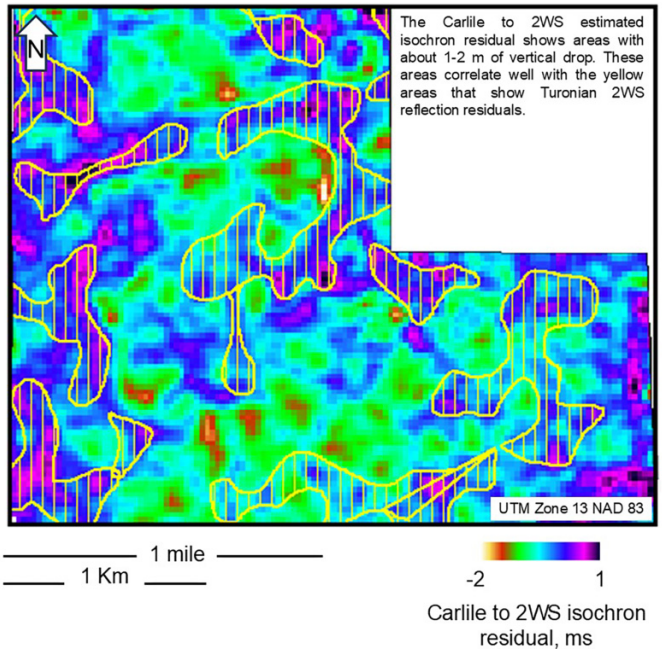

Fig. 26. The Second White Specks (2WS) to Westgate isochron residual map shows pairs of thick and thin areas adjacent to the low residual 2WS areas.

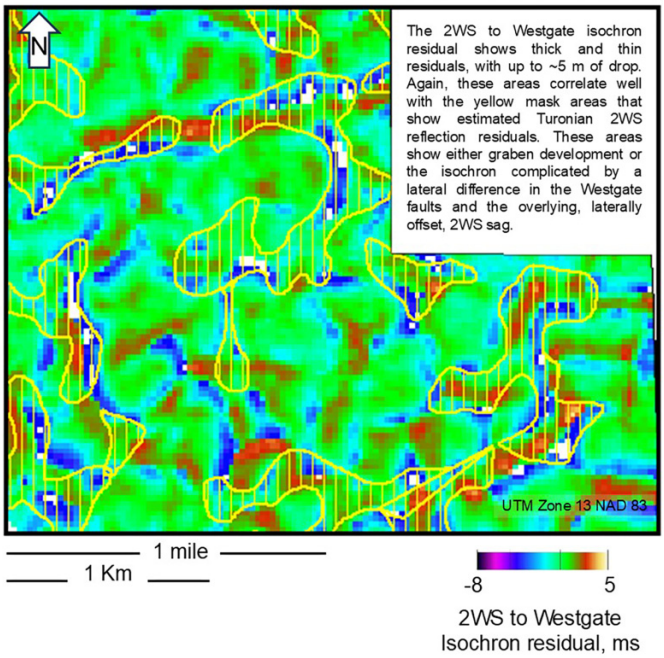

Fig. 27. Westgate to Viking isochron residuals. This map outlines the Westgate faulting well. Again, these grabens correlate to the yellow hashed area, showing residual Turonian Second White Specks (2WS) low areas.

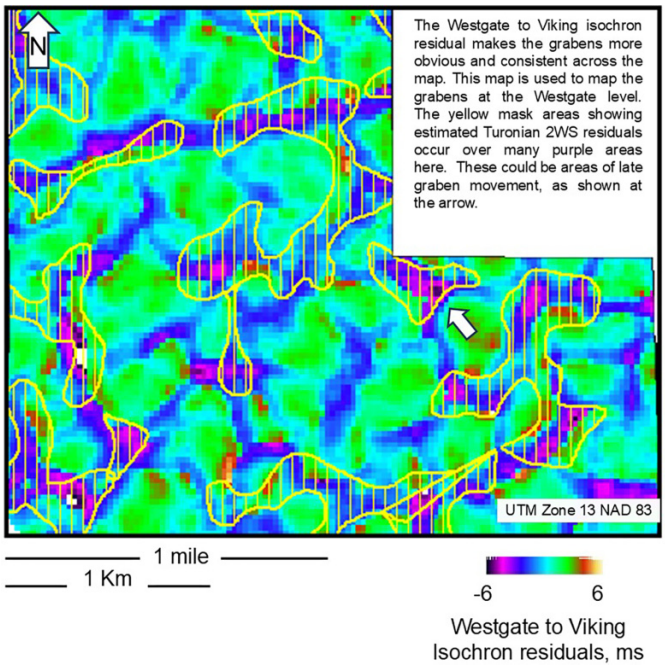

acteristic to consider, along with other evidence, such as the seismic data presented here for PFS identification.

It is unknown whether the Westgate Formation faults are open or closed in the subsurface. Indications of production surrounding the Success, Saskatchewan area, show that the faults are closed. There is no known hydrocarbon production from Westgate Formation shales. However, at Success, Saskatchewan, the adjacent underlying Viking reservoir is productive (~40 km southeast at 8-30-13-13W4, for example). Viking Formation production history plots do not show adverse production characteristics because of open fractures in the Westgate Formation.

As society continues to seek suitable candidates for carbon sequestration, at least two areas have been considered: areas where the Westgate Formation or the Mowry Shale (in the US) was deposited. The Aquistore site stores CO_2 near Estevan, Saskatchewan, in deeper formations near the Precambrian basement (White et al. 2014). South of this location, the Albian/Cenomanian Dakota Group in North Dakota (time equivalent to the Viking Formation) has been recognized as a potential storage site for CO_2 carbon sequestration (Gorecki et al. 2009). Before work such as hydraulic fracturing is considered in other areas, the Westgate Formation should be analyzed for in situ strength, especially if the target zone is adjacent formations.

Fracture enhancement of Second White Speckled Shale Formation reservoirs

Post-Turonian-time graben formation in the Albian Westgate Member is presented as a model for fracture creation that could enhance shallower Second White Speckled Shale Formation reservoirs. About half of the graben movement discussed here occurred after the deposition of the Turonian 2WS strata; see Fig. 28. If these strata were lithified, the downward movement could cause fracturing, enhancing permeability. Marion and Cheadle (2017) recognized that developing a fracture prediction model is essential for this reservoir, as natural fracture networks are essential to the production characteristics. This timing of the Westgate fracturing is presented here as this model. These shallower reservoirs are generally low porosity reservoirs. Any permeability enhancement by late Westgate Formation faulting might enhance the economic recovery of hydrocarbons from these reservoirs. This model should apply to homotoaxially equivalent strata in the USA, specifically the Greenhorn Formation above the homotaxially equivalent Mowry Shale Formation in the USA

Comments on the faulting observed here

Consider these general comments that do not require extensive discussion. These are observations made during this study:

- The seismic data presented here image a PFS. However, most PFS in the literature have many faulted seismic reflections; this PFS may be one of the few defined essentially by faulting observed on only one seismic reflection. However, consistent seismic reflections in the strata above the faulted reflection allow for the timing of the graben dissolution here.
- The dissolution model presented here is a simple model using a process that has a scant discussion in the academic community: volcanogenic strata can undergo rheological change as the strata are altered, such as the illitization of

Fig. 28. A summary of the observed downward movement, as estimated by the residual maps. Wellbore analyses can determine the timing of the faulting in the Westgate strata. 2WS, Second White Specks.

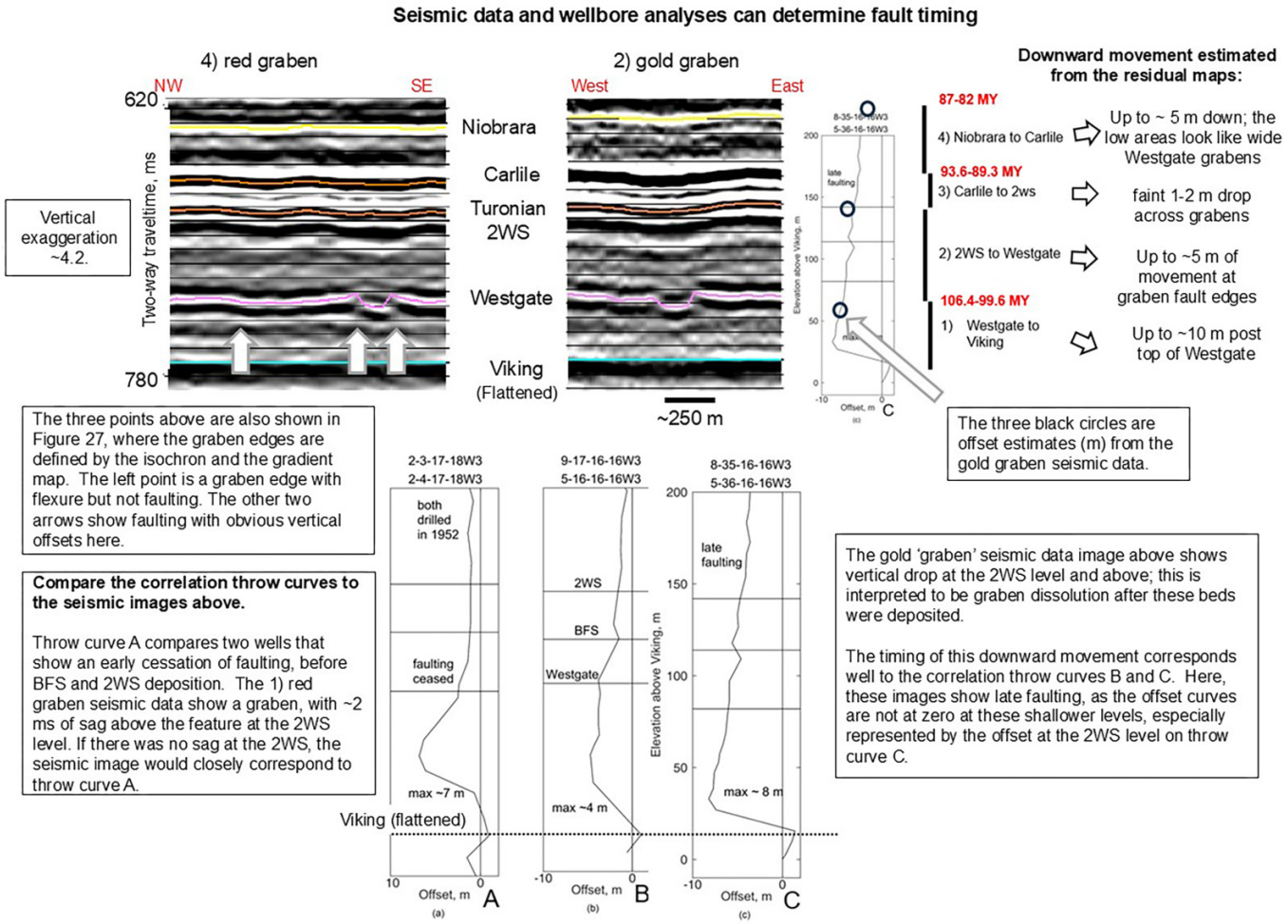

smectite presented here. The model is simple; others are encouraged to test the shear-thinning model for PFS creation in their study area.

- It is believed faulting in the Westgate Formation is fractal. This means the fracturing and faulting occur at scales ranging from the mesoscale to the microscopic scale. At the mesoscale, the grabens are defined by faults with strike lengths of 100 m or more. At the microscopic scale, the faulting and fracturing observed at outcrop and in core analyses might show fractal mesoscale fault characteristics. Others have recognized the fractal characteristics of PFS (Adiotomre et al. 2010).
- The faulting along the graben edges shows lateral variations in vertical offset; consider Fig. 19. The color variations along any fault trace show variations in fault characteristics, including lateral cessation of faulting. If PFSs are fractal phenomena, the lateral offset change from 10 to 0 m of vertical throw implies a complicated area of faulting and fracturing in that lateral area. Tewksbury et al. (2014) made a similar correlation while examining the outcrop of the Khoman Formation PFS in Egypt. Tewksbury et al. (2014) correlated small-scale features, such as tight fault clusters and vein systems to the macroscopic characteristics of PFS.
- Tewksbury et al. (2014) also related pressurized fluids to faulting during initial PFS formation and evolution. The same process is possible here, with illitization being more possible in faulted or fractured areas that could distribute K+ ions to smectite strata in the Westgate Formation.
- The importance of the high-silica content sources for the strata is still under investigation. This includes the formation of authigenic silica and detrital quartz, for example, or the transition from opal-A to opal-CT. Current work focuses on the estimates of illite transformation and the subsequent production of SiO_2 in fractal PFS fault systems. Other work is considering silica in a gel form in the WIS.

The Mowry Shale

The Mowry Shale, homotaxial equivalent to the Westgate Formation, south of Canada into the USA, could also host PFS. Extensive faulting and fracturing, consistent with PFS measurement, have been reported in the Powder River Basin in Montana and Wyoming (Anna and Cook 2008). Applying a simple PFS model to the Mowry might enhance understanding of faulting processes in such areas. However, this could

Fig. 29. A crossplot of the three residual maps summarized together and then cross-plotted against the Westgate to Viking isochron residuals. The almost 1:1 correlation shows that the individual regional maps did not remove the residual effect of the vertical movement. This should be obvious by inspection of the regional maps presented here. 2WS, Second White Specks.

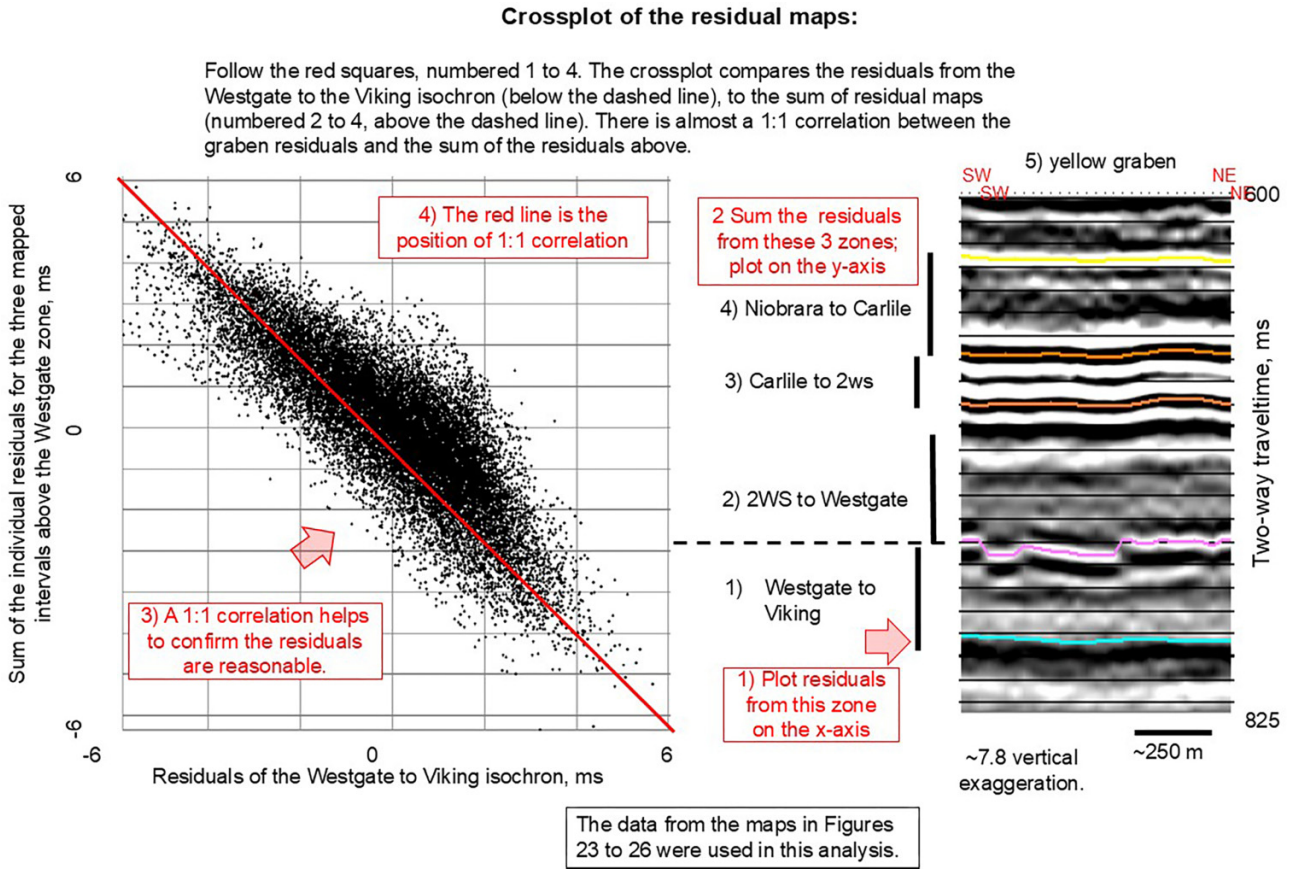

be difficult, as there is extensive faulting in areas such as the Powder River Basin, including large-scale tectonic processes. While beautiful to observe, PFS faulting can be subtle. However, recognizing subtle PFS formation could enhance understanding of Mowry Shale hydrocarbon reservoirs. This enhancement could have economic ramifications; Anna and Cook (2008) report on extensive production from the Mowry (over 1.2 billion barrels of oil).

Westgate Formation as proof of two polygonal fault system models

The polygonal faulting in the Westgate Formation can be related to a simple PFS formation model. Consider Fig. 30, showing a model of shear-thinning, bed dissolution, and graben formation. This describes a simple PFS formation model. The change in rheological properties of volcanogenic strata is germane to the initiation and propagation of PFS. The Westgate Formation contains smectite; smectite can undergo illitization. This process can occur at shallow depths and in fault gouge (Casciello et al. 2011). When this occurs, it is believed that something under-reported in the literature occurs—illite has shear-thinning rheology (Jeong 2012, for example). When this occurs, the illite can dissolve. It is believed that illitization could occur in areas such as fractures if the fractures allow for the movement of K+ ions or are the location for temperature increases (both promote illitization). Illitization, shear-thinning, and bed dissolution could start this PFS.

Philippe et al. (2011) examined the shear-thinning behavior of montmorillonite and beidellite under shear, recognizing that an external shear force could induce shear-thinning. The volcanic activity that produced the Westgate Formation strata may have created large earthquakes that could be a source of shear energy to affect in situ montmorillonite and/or beidellite enough to induce shear-thinning and subsequent dissolution.

The Mowry Shale has been identified to contain many bentonite beds, with as many as 55 beds in some areas (Heathman 1939). The properties of the beds determine shear-thinning and shear-thickening properties. It is important to note that the transformation of bentonite, smectite, or montmorillonite to beidellite or illite is a change from shear-thickening to shear-thinning properties for the strata. These changes can induce weakness in the strata. It is believed that this occurred throughout the WIS, initiating PFSs over a large area.

Dusenkova et al. (2013) examined the rheological properties of Latvian illite clays. The presence of soluble salts influenced the shear-thinning properties of the clays. Similarly, changes in salt concentrations might have affected the rheological properties of illite in the Westgate Formation.

Fig. 30. A simple model for forming the Westgate polygonal fault system is presented. Volcanic strata are deposited (Bloch et al. 1999); smectite beds can be illitized (Casciello et al. 2011, and Jeong et al. 2012), starting shear-thinning, bed dissolution, subsequent graben formation, and polygonal fault system (PFS) occurrence. WIS, Western Interior Seaway.

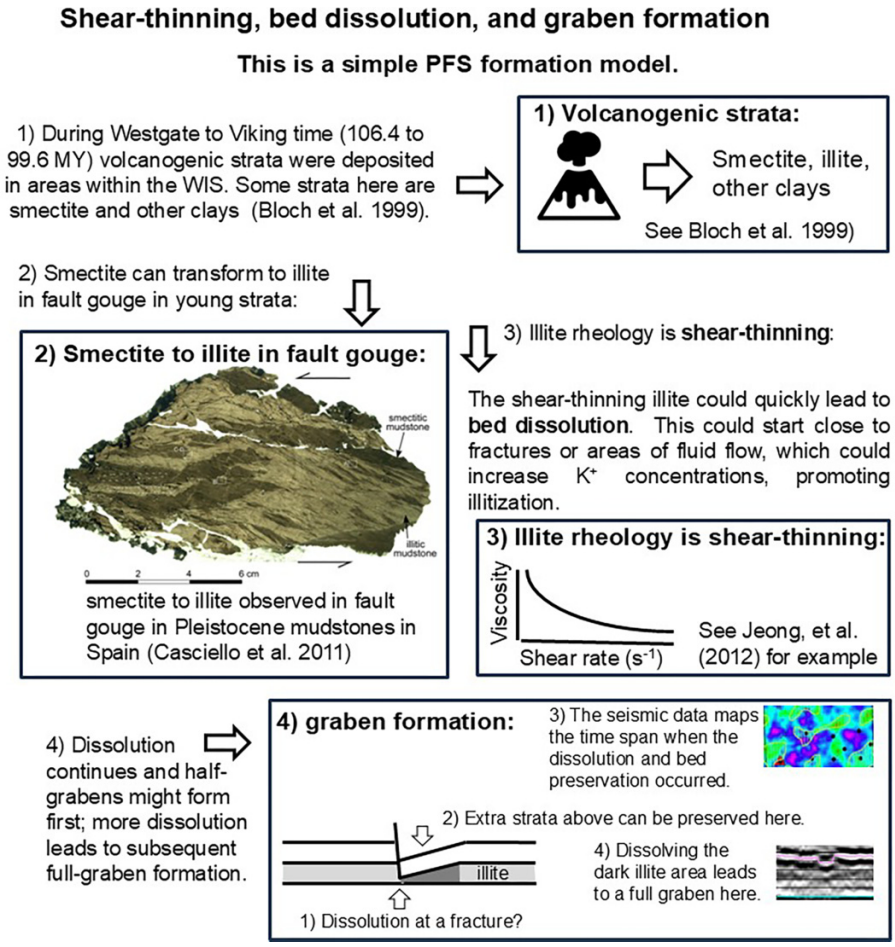

Dellisanti et al. (2008) examined the role of tectonic shear strain and how it affects the transformation of mixed-layer I–S to illite in fault zones. Key to the model is the shearing of strata and the presence e of K+ ions. The transformation results in more illite, a shear-thinning clay. This model is believed to apply here.

Another initiator of PFS is believed to be the densification of high-content silica strata. St-Onge (under review) shows that the densification of SiO_2 particles to over 60% concentration by volume could lead to a glass transition and fracturing. The Mowry Shale has up to 84% silica content in some areas (Rubey 1927; Bramlette 1946; Longman et al. 2019). It is believed that this densification, glass transition, and fracturing could have occurred in the high-silica strata while shear-thinning and shear-thickening changes were occurring in the clay strata. Finite element modeling of these strata might provide a better understanding of these processes.

Summary and ramifications of the Westgate Formation PFS

Polygonal faulting in the Westgate Formation has been presented using seismic data and geological wellbores, and these two datasets have been integrated here. The observations are consistent with two hypotheses for polygonal fault development. The potential densification of high-silica strata in the Westgate Formation could have caused PFS development, consistent with St-Onge (under review). Another explanation for the PFS development could have been the simple dissolution of one of many bentonite beds in the shales. For example, a change in ion characteristics could have caused deeper shear-thinning in strata, as what occurs when shear-thickening smectite alters into shear-thinning illite, for example. When this occurs, the shear-thinning smectite transforms into a shear-thinning bed. This transformation could induce weakness, creating faulting and fracturing over a large area, as discussed by St-Onge (under review).

Four primary points should be made regarding the ramifications of a Westgate Formation PFS:

1. PFS formation in strata could be caused by illitization and subsequent shear-thinning and dissolution of deeper strata. This model explains faulting and fracturing observed in the wellbore, at outcrop, and on 3D seismic datasets imaging the Westgate Formation.

2. The Westgate Formation bulk rock properties may differ within a PFS, as the zone appears to have undergone extensive faulting, fracturing, and potential bed dissolution. Weakness induced by these processes should be considered when hydraulic fracturing adjacent strata.
3. The drilling density, outcrop occurrence, and seismic database imaging of the Westgate Formation make it an excellent candidate for further study of PFS formation.
4. Faults that occurred late in the Westgate Formation (and homotaxial equivalents) deposition may have induced faulting and fracturing in shallower tight gas reservoirs; this could enhance their productivity and should be investigated further.

Conclusions

A previously undescribed PFS is interpreted to occur within the Westgate Formation deposited within the WIS. The formation is host to a succession of fine-grained siliceous sediments consistent with PFS occurrence. Graben-bounding faults are mapped in an intricate array of coalesced narrow and shallow grabens. Seismic data and well-log interpretation date the fault timing to after 270 000 years of the start of Westgate Formation sediment deposition in ~15 m or more of compacted sediment thickness (~106 MY). Seismic data map graben dissolution creating accommodation space extra for the section to be preserved above the grabens in strata as young as the Niobrara Formation (~82 MY). The graben distribution is attributed to bed illitization and subsequent shear-thinning and bed dissolution of these strata. A simple isopach analysis of correlative Westgate Formation marker beds should help confirm PFS areas outside this study's bounds, along with other evidence, such as seismic data. The implications for an extensive PFS in the Lower Cretaceous include reservoir models for seal integrity for underground sequestration or late faulting that could enhance porosity in shallower fractured reservoirs such as the Second Whites Speckled Shale Formation reservoirs.

Acknowledgements

TGS Seismic and Ms. Rachel Binnion are thanked for their generous contribution in allowing the scientific use of the Leinan and Success 3D seismic datasets. SeisWare is thanked for the generous contribution of its seismic interpretation software for this study.

Article information

History dates

Received: 15 June 2024
Accepted: 21 October 2024
Accepted manuscript online: 6 November 2024
Version of record online: 3 March 2025

Copyright

Data availability

The primary research data are seismic data that can be licensed through TGS, the data owners. Visit www.tgs.com to find a representative to help you with a potential data review.

Author information

Author ORCIDs

Andy St-Onge https://orcid.org/0000-0003-4396-0637

Author contributions

Conceptualization: AS
Data curation: AS
Formal analysis: AS
Investigation: AS
Methodology: AS
Resources: AS
Validation: AS
Visualization: AS

Competing interests

The author declares there are no competing interests.

Supplementary material

Supplementary data are available with the article at https://doi.org/10.1139/cjes-2024-0088.

References

Adiotomre, E., Finch, E., Gawthorpe, R., and Huuse, M. 2010. Fractal and spatial analysis of polygonal fault systems case study: shallow slope section offshore Angola West Africa, AAPG Search and Discovery Article. Available from https://www.searchanddiscovery.com/pdfz/abstracts/pdf/2010/african_regional/abstracts/ndx_adiotomre.pdf.html [accessed 3 October 2023].

Anna, L.O., and Cook, T.A. 2008. Assessment of the Mowry Shale and Niobrara Formation as continuous hydrocarbon systems, Powder River Basin, Montana, and Wyoming, American Association of Petroleum Geologists Section Conference, July 9, 2008, Denver, Colo.: US Geological Survey Open-File Report 2008–1367, 1 sheet.

Al-Hashemi, HM.B, and Al-Amoudi, OS.B. 2018. A review on the angle of repose of granular materials. Powder Technology, **330**: 397–417. ISSN 0032-5910. doi:10.1016/j.powtec.2018.02.003.

Bloch, J., Schröder-Adams, C., Leckie, D., McIntyre, D., Craig, J., and Staniland, M. 1993. Revised stratigraphy of the lower Colorado Group (Albian to Turonian), western Canada. Bulletin of Canadian Petroleum Geology, **41**: 325–348. Available from https://api.semanticscholar.org/CorpusID:129248667 [accessed November 2020].

Bloch, J., Schröder-Adams, C., Leckie, D., Craig, J., and McIntyre, D. 1999. Sedimentology, micropaleontology, geochemistry, and hydrocarbon potential of shale from the Cretaceous Lower Colorado Group in western Canada. Geological Survey of Canada Bulletin 531. Available from http://geoscan.nrcan.gc.ca/starweb/geoscan/servlet.starweb?path=geoscan/fulle.web&search1=R=211004 [accessed November 2016].

Bramlette, M.N. 1946. The Monterey Formation of California and the origin of its siliceous rocks': US Geol. Survey Prof. Paper 212, 57p. Available from https://pubs.usgs.gov/publication/pp212 [accessed 15 June 2024].

Caldwell, W.G.E., and North, B.R. 1984. Cretaceous stage boundaries in the southern interior plains of Canada. Bulletin of the Geological Society of Denmark, **33**: 57–69. doi:10.37570/bgsd-1984-33-05. Available from http://2dgf.dk/xpdf/bull33-01-02-57-69.pdf [accessed November 2016].

Caldwell, W.G.E., Diner, R., Eicher, D.L., Fowler, S.P., North, B.R., Stelck, C.R., and von Holdt Wilhelm, L. 1993. Foraminiferal biostratigraphy of Cretaceous marine cyclothems. *In* Evolution of the Western Interior Basin. *Edited by* W.G.E. Caldwell and E.G. Kauffman. Geological Association of Canada, Special Paper 39. pp. 477–520.

Cartwright, J. 2011. Diagenetically induced shear failure of fine-grained sediments and the development of polygonal fault systems. Marine and Petroleum Geology, **28**(2011): 1593–1610. doi:10.1016/j.marpetgeo.2011.06.004.

Cartwright, J., and Dewhurst, D. 1998. Layer-bound compaction faults in fine-grained sediments. Geological Society of America Bulletin, **10**(10): 1242–1257. doi:10.1130/0016-7606(1998)110⟨1242:LBCFIF⟩2.3.CO; 2.

Cartwright, J.A., and Lonergan, L. 1996. Volumetric contraction during the compaction of mudrocks: a mechanism for the development of regional-scale polygonal fault systems. Basin Research, **8**: 183–193, doi:10.1046/j.1365-2117.1996.01536.x.

Cartwright, J.A., Huuse, and Aplin, M.C. 2007. Seal bypass systems. AAPG Bulletin, **91**(8): 1141–1166. doi:10.1306/04090705181.

Casciello, E. Cosgrove, J.W., Cesarano, M., Romero, E., Queralt, I., and Vergés, J. 2011, Illite–smectite patterns in sheared Pleistocene mudstones of the Southern Apennines and their implications regarding the process of illitization: a multiscale analysis. Journal of Structural Geology, **33**(11): 1699–1711. ISSN 0191-8141. doi:10.1016/j.jsg.2011.08.002.

Catuneaunu, O., Sweet, A., and Miall, A. 2000. Reciprocal stratigraphy of the Campanian-Paleocene Western Interior of North America. Sedimentary Geology, **134**(2000): 235–255. doi:10.1016/S0037-0738(00)00045-2.

Christopher, J.E., Yurkowski, M., Nicolas, M., and Bamburak, J. 2006. The Cenomanian–Santonian Colorado formations of eastern and southern Saskatchewan and southwestern Manitoba. *In* Saskatchewan and Northern Plains Oil & Gas Symposium 2006. *Edited by* C.F. Gilboy and S.G. Whittaker. Saskatchewan Geological Society Special Publication 19. pp. p299–p318. Available from https://www.manitoba.ca/iem/geo/willistontgi/downloads/christopher_et_al_colorado_paper.pdf [accessed 14 June 2024].

Cosgrove, J. 2001. Hydraulic fracturing during the formation and deformation of a basin: a factor in the dewatering of low-permeability sediments. AAPG Bulletin, **85**(4): 737–748. doi:10.1306/8626C997-173B-11D7-864500010C1865D.

Dellisanti, F., Pini, G.A., Tateo, F., and Baudin, F. 2008. The role of tectonic shear strain on the illitization mechanism of mixed-layers illite–smectite. A case study from a fault zone in the Northern Apennines, Italy. International Journal of Earth Sciences, **97**(3): 601. doi:10.1007/s00531-007-0180-4.

Dewhurst, D., Cartwright, J., and Lonergan., L. 1999. Three-dimensional consolidation of fine-grained sediments. Canadian Geotechnical Journal, **36**: 355–362. doi:10.1139/t98-101.

Dusenkova, I., Stepanova, V., Vecstaudza, V., Jana, L., Vitalijs, Malers, J., and Berzina-Cimdina, L. 2013. Rheological properties of Latvian illite clays. Acta Geodynamica et Geomaterialia, **10**(4): 459–464. doi:10.13168/AGG.2013.0046.

Finn, T.M. 2021, Stratigraphic cross sections of the Mowry Shale and associated strata in the Wind River Basin, Wyoming: US Geological Survey Scientific Investigations Map 3476, 1 sheet, 14-p. pamphlet. doi:10.3133/sim3476.

French, KL., Birdwell, JE., and Lillis, PG. 2022. Geochemistry of the Cretaceous Mowry Shale in the Wind River Basin, Wyoming. Geological Society of America Bulletin, **135**(7–8): 1899–1922. doi:10.1130/B36382.1.

Gorecki, C., Sorensen, J., Steadman, E., and Harju, J. 2009. CO_2 storage risk minimization through systematic identification and assessment of faults: a Williston Basin case study. Energy Procedia, **1**(2009): 2887–2894. doi:10.1016/j.egypro.2009.02.063.

Goulty, N. 2008. Geomechanics of polygonal fault systems: a review. Petroleum Geoscience, **14**(4): 389–397. doi:10.1144:1354-079308-781.

Goulty, N., and Swarbrick, R. 2005 Development of a polygonal fault system: a test of hypotheses. Journal of the Geological Society, London, **162**: 587–590. doi:10.1144:0016-764905-004.

Hay, D., Banks, C., and Prior, G. 2012. Measured outcrop sections T79-R17W4-01 (Stony Rapids) and T81-R17W4-01 (Pelican Cliffs) of the Pelican, Westgate, Fish Scales and Belle Fourche Formations near Stony Rapids, Athabasca River, Northeastern Alberta (NTS 83P/15 and NTS 84A/02). Energy Resources Conservation Board, Alberta Geological Survey. Available from http://ags.aer.ca/document/OFR/OFR_2012_02.PDF [accessed 7 November 2016].

Heathman, J.H. 1939. Bentonite in Wyoming: Wyoming. Geol. Survey Bull. 28. 5 figs. pp. 1–20. Available from https://www.wsgs.wyo.gov/products/wsgs-1939-b-28.pdf [accessed 15 June 2023].

Jeong, S.W., Locat, J., and Leroueil, S. 2012, The effects of salinity and shear history on the rheological characteristics of illite-rich and Na-montmorillonite-rich clays. Clays and Clay Minerals, **60**: 108–120, doi:10.1346/CCMN.2012.0600202.

Leckie, D.A., Schröder-Adams, C.J., and Bloch, J. 2000. The effect of paleotopography on the late Albian and Cenomanian sea-level record of the Canadian Cretaceous Interior Seaway. Geological Society of America Bulletin, **112**: 1179–1198. doi:10.1130/0016-7606(2000) 112⟨1179:TEOPOT⟩2.0. CO; 2.

Marion, K., and Cheadle, B. 2017. Solving the Second White Specks: integrating petrophysics and allostratigraphy to find sweet spots. *In* CSEG Geoconvention, Calgary, 2017. Available from https://geoconvention.com/wp-content/uploads/abstracts/2017/290_GC2017_Solving_the_Second_White_Specks.pdf [accessed 3 October 2024].

Longman, MW., Drake, WR., Milliken, KL., and Olson, TM. 2019. Chapter 4: A Comparison of Silica Diagenesis in the Devonian Woodford Shale (Central Basin Platform, West Texas) and Cretaceous Mowry Shale (Powder River Basin, Wyoming), AAPG Special Volumes, Memoir 120: Mudstone Diagenesis: Research Perspectives for Shale Hydrocarbon Reservoirs, Seals, and Source Rocks, 2019. pp. 49–67. doi:10.1306/13672210M12163.

McNeil, D.H., and Caldwell, W.G.E. 1981. Cretaceous Rocks and Their Foraminifera in the Manitoba Escarpment. Geological Assoc. of Canada Spec. Pap. 21, 439p.

Milliken, KL., and Olson, T. 2017. Silica diagenesis, porosity evolution, and mechanical behavior in siliceous mudstones, Mowry Shale (Cretaceous), Rocky Mountains, USA. Journal of Sedimentary Research, **87**(4): 366–387. doi:10.2110/jsr.2017.24.

Pedersen, K., Schröder-Adams, C., and Vorobieva, O. 2001. Sedimentary Architecture of the Bow Island Formation, Southwestern Alberta, Canada. Canadian Society of Petroleum Geology, CSPG Convention 2001, Calgary.

Pedersen, P.K. 2004. Shallow gas research project in southwestern Saskatchewan: Revised lithostratigraphy of the Colorado Group and reservoir architecture of the Belle Fourche and Second White Specks in the Senate Pool. *In* Summary of Investigations 2004, Volume 1, Saskatchewan Geological Survey, Sask. Industry Resources, Misc. Rep. 2004-4.1, CD-ROM, Paper A-16, 15p.

Philippe, A., Baravian, C., Imperor-Clerc, M., De Silva, J., Papineau, E., Bihannic, I., et al. 2011. Rheo-SAXS investigation of shear-thinning behavior of very anisometric repulsive disc-like clay suspensions. Journal of Physics: Condensed Matter, **23**(19): 194112. doi:10.1088/0953-8984/23/19/194112.

Prokoph, A., and Atgerberg, F.P. 1999. Detection of sedimentary cyclicity and stratigraphic completeness by wavelet analysis: an application to Late Albian cyclostratigraphy of the Western Canada Sedimentary Basin. Journal of Sedimentary Research, **69**(4): 862–875. doi:10.2110/jsr.69.862.

Roberts, D., Crook, A., Cartwright, J., and Profit, M. 2015. Investigating the Evolution of Polygonal Fault Systems Using Geomechanical Forward Modeling. 49th US Rock Mechanics /Geomechanics Symposium held in San Francisco, CA, USA, 28 June-1 July 2015, ARMA-2015-342.

Roberts, L., and Kirschbaum, M. 1995. Paleogeography of the Late Cretaceous of the Western Interior of Middle North America- Coal distribution and sediment accumulation. USGS Professional Paper 1561, US Government Printing Office. Available from http://pubs.usgs.gov/pp/1561/report.pdf [accessed April 2016].

Rubey, W. 1927. Origin of the siliceous Mowry Shale of the Black Hills Region. Available from https://pubs.usgs.gov/pp/0355/report.pdf [accessed 15 June 2024].

Schröder-Adams, C.J., Leckie, D., Bloch, J., Craig, J., McIntyre, D., and Adams, P. 1996. Paleoenvironmental changes in the Cretaceous (Albian to Turonian) Colorado Group of western Canada: microfossil, sedimentological and geochemical evidence. Cretaceous Research, **17**: 311–365, doi:10.1006/cres.1996.0022.

St-Onge, A. 2017. A Late Cretaceous polygonal fault system in central North America. Geological Society of America Bulletin, **129**(5–6): 582–593. doi:10.1130/B31582.1.

Schultz, L., Tourtelot, H., Gill, J., and Boerngen, J. 1980. Composition and properties of the Pierre Shale and equivalent rocks, northern Great Plains region. USGS Professional Paper 1064. Available from http://pubs.usgs.gov/pp/1064b/report.pdf [accessed April 2016].

Tewksbury, BJ., Hogan, J.P., Kattenhorn, S.A., Mehrtens, C.J., and Tarabees, E.A. 2014. Polygonal faults in chalk: insights from extensive exposures of the Khoman Formation. Geology, **42**(6): 479–482. doi:10.1130/G35362.1.

TGI Williston Basin Working Group. 2008. Cretaceous Westgate Formation: isopach; Manitoba Science, Technology, Energy and Mines, Manitoba Geological Survey, Stratigraphic Map SM2008-KW-I, scale 1:1000 000. Available from www.WillistonTGI.com [accessed December 2024].

Watterson, J., Walsh, J.J., Nicol, A., Nell, P.A.R., and Bretan, P.G. 2000. Geometry and origin of a polygonal fault system. Journal of the Geological Society, **157**: 151–162. doi:10.1.1.112.5134.

White, D., Roach, L., Roberts, B., and Daley, T. 2014. Initial results from monitoring at the Aquistore CO_2 storage site, Saskatchewan, Canada. Energy Procedia, **63**(2014): 4418–4423. doi:10.1016/j.egypro.2014.11.477. Available from http://www.osti.gov/pages/servlets/purl/1206350 [accessed November 2016].

Williams, G.D., and Stelck, C.R. 1975. Speculations on the Cretaceous Palaeogeography of North America. *In* The Cretaceous system in the Western Interior of North America: Geological Association of Canada Special Paper, No. 13. QE685.C88. *Edited by* W.G.E. Caldwell. pp. 1–20.

Wong, R.C.K., Kumar, D., and Gautam, R. 2011. Geotechnical properties of bentonite seams—its effects on casing integrity under steam injection in Cold Lake, Alberta. Canadian Geotechnical Journal, **48**(10): 1551–1569. doi:10.1139/t11-058.

Zhang, H. 2006. Allostratigraphy of the Shaftesbury Formation, northern Alberta and northeastern British Columbia: Responses to eustatic and tectonic controls. Master of Science thesis, University of Western Ontario. 237p.

Zhang, N. 2015. Natural fracture systems in Mowry Shale outcrops, Bighorn Basin, Wyoming. Iowa State University. Available from https://dr.lib.iastate.edu/entities/publication/969f60b7-ec64-40e0-938f-3104b50bf3b0/full [accessed 15 June 2024].

Zourob, A. 2020. Stratigraphic studies of Late Albian strata. northeastern Alberta. PhD thesis, University of Western Ontario. Available from https://ir.lib.uwo.ca/etdhttps://ir.lib.uwo.ca/etd/6805 [accessed December 2024].